

# Probability of Detecting a Planetary Companion during a Microlensing Event

S. J. Peale

*Dept. of Physics  
University of California  
Santa Barbara, CA 93106  
peale@io.physics.ucsb.edu*

## ABSTRACT

The averaged probability of detecting a planetary companion of a lensing star during a microlensing event toward the Galactic center when the planet-star mass ratio  $q = 0.001$  is shown to have a maximum exceeding 10% at an orbit semimajor axis near 1.5 AU for a uniform distribution of impact parameters. This peak value is somewhat lower than the maximum of 17% obtained by Gould and Loeb (1992), but it is raised to more than 20% for a distribution of source-lens impact parameters that is determined by the efficiency of event detection. Although these probabilities, based on a signal to noise (S/N) detection criterion, are model and assumption dependent, the fact that they change in predictable ways as functions of the orbit semimajor axes but remain robust for plausible variations of all the relevant galactic parameters implies that they are representative of real values. In addition, the averaging procedures are carefully defined, and they determine the dependence of the detection probabilities on several properties of the Galaxy. The probabilities for other planet-star mass ratios can be estimated from an approximate scaling of  $\sqrt{q}$ . A planet is assumed detectable if the perturbation of the single lens light curve exceeds  $2/(S/N)$  sometime during the event, where it is understood that at least 20 consecutive photometric points during the perturbation are necessary to confirm the detection.  $S/N$  is the instantaneous value for the amplified source. Two meter telescopes with 60 second integrations in I-band with high time resolution photometry throughout the duration of an ongoing event are assumed. The probabilities are derived as a function of semimajor axis  $a$  of the planetary orbit, where the peak probability occurs where  $a$  is approximately the mean Einstein ring radius of the distribution of lenses along the line of sight. The probabilities remain significant for  $0.6 \lesssim a \lesssim 10$  AU. Dependence of the detection probabilities on the lens mass function, luminosity function of the source stars as modified by extinction, distribution of source-lens impact parameters, and the line of sight to the source are also determined, and the probabilities are averaged over the distribution of the projected position of the planet onto the lens plane, over the lens mass function, over the distribution of impact parameters, over the distribution of lens and sources along the line of sight and over the I-band luminosity function of the sources adjusted for the source distance and extinction. The probability for a particular impact parameter and particular source  $I$  magnitude

but averaged over remaining degenerate parameters also follows from the analysis. In this latter case, the extraction of the probability as a function of  $a$  for a particular  $q$  from the empirical data from a particular event is indicated.

## 1. Introduction

There are several searches for extrasolar planets using radial velocity techniques that together have discovered more than 50 planets with minimum masses less than 13 Jupiter masses ( $M_J$ ) (*e.g.*, Marcy, Cochran & Mayor 2000). Astrometric searches so far have been unsuccessful, but new astrometric satellites (Full-sky Astrometric Mapping Explorer (FAME), Space Interferometry Mission (SIM), Global Astrometric Interferometer for Astrophysics (GAIA)) with precisions approaching micro-arcseconds (Lattanzi *et al.* 2000) and the Keck Interferometer (Swain *et al.* 2000), which may do almost as well, should soon add additional planets. Transit searches have yet to discover a new planet, but a planet discovered by radial velocity techniques has been successfully observed in transit (Charbonneau *et al.* 2000; Henry *et al.* 2000). Continuing transit searches should lead to more discoveries. All of these search techniques except astrometry favor the discovery of close, massive planets, and all are restricted to planetary periods that are only slightly greater than the time the program has been in operation or less. The one astrometric program with a long time base (Gatewood, 1991) but no detected planets has too few target stars to be definitive. The program initiated by G. Marcy, while having a long time base, has reached the necessary precision of 3 m/sec to detect distant Jupiters and Saturns only a few years ago, but the current program has a sufficient number of stars to constrain the statistics of distant Jupiters similar to the one in our own solar system in about 5 years (G. Marcy, D. Fischer, private communications, 2000).

Mao and Paczyński (1991) pointed out that a planetary companion of a star acting as a gravitational lens amplifying the light of a more distant star (microlensing) could perturb the otherwise smooth light curve in an easily observable way and thereby reveal its presence. There are many examples in the literature of microlensing light curves perturbed by a planet along with descriptions of the single lens amplification (*e.g.* Peale, 1997). The information about the planet from the perturbed light curve alone is usually limited to the planet-star mass ratio  $q$  and the projected separation of the planet from the star in terms of the Einstein ring radius,

$$R_E = \sqrt{\frac{4GM}{c^2} \frac{D_{OL}(D_{OS} - D_{OL})}{D_{OS}}},$$

$$= \sqrt{\frac{4GMD_8}{c^2} \frac{z(\zeta - z)}{\zeta}}, \quad (1)$$

where  $G$  is the gravitational constant,  $M$  is the mass of the lensing star,  $c$  is the velocity of light,  $D_{OL}$  and  $D_{OS}$  are the observer-lens and observer-source distances respectively,  $z = D_{OL}/D_8$ , and  $\zeta = D_{OS}/D_8$  with  $D_8 = 8$  kpc being the distance to the center of the Galaxy. Statistically, the projected star-planet separation is a measure of the semimajor axis of the planetary orbit (Peale, 1997).

Part of the search for microlensing events has been directed toward the Galactic bulge, where the high concentration of stars in the telescope field allowed a reasonable rate of event detection and where more than 300 events have, in fact, been detected (<http://darkstar.astro.washington.edu>; <http://bulge.princeton.edu/ogle/>; <http://www.lal.in2p3.fr/recherche/eros/erosa.html>). Gould and Loeb (1992) showed that the probability of detecting a planet with  $q = 0.001$  during a microlensing event approached 17% if the planet's projected separation from the star was comparable to the Einstein ring radius  $R_E$ . A planet was assumed detectable if the perturbation exceeded 5% of the instantaneous flux of the unperturbed single lens light curve. The probability was averaged over a uniform distribution of lenses along the line of sight (LOS) to a source at the Galactic center. The averaged position of the lens was thus halfway to a source at the galactic center, where  $R_E \approx 4.1$  AU for a solar mass star meant that a Jupiter would have nearly the maximum probability of detection.

This high probability of detecting a planetary companion during a microlensing event generated an enthusiastic advocacy for establishing an intensive, dedicated microlensing search program from the ground (Beichman *et al.*, 1996). Initially more modest microlensing search programs (PLANET (Probing Lensing Anomalies NETwork), Albrow *et al.* 1998, and MPS (Microlensing Planet Search), Rhie *et al.* 2000) have progressed to different degrees of maturity and are beginning to place meaningful constraints on the occurrence of Jupiter mass planets around M dwarfs (Albrow *et al.* 2000). The enthusiasm was reinforced by the special status noted for very high magnification events, where the probability of detecting a planet is unity for a range of projected planet-star separations in the lensing zone surrounding the Einstein ring radius (Griest and Safizadeh 1998). The advantage of a microlensing search over the other search techniques

is that the planets in long period orbits could be discovered without watching for a decade, and statistics would start accumulating immediately. The disadvantage, of course, is that the lenses are so distant that there could be no followup studies of the planet after the event. But the knowledge of the frequency of occurrence of planetary systems and the need to know these statistics rapidly for planning future planetary search missions are sufficient to keep microlensing as a most important search technique.

This work develops a probability of planet detection during microlensing events that is based on the photometric signal-to-noise ratio ( $S/N$ ) for the amplified source, with the goal of determining the dependence of this probability on plausible variations in Galactic parameters while establishing robust averaging techniques over the distributions of Galactic parameters. The probability is determined as a function of the planet orbit semimajor axis for a planet-star mass ratio of  $q = 0.001$ , and an approximate scaling law for other mass ratios is indicated. From some points of view, it might be more desirable to express the probabilities for planetary masses instead of the planet-star mass ratio. However, the microlensing calculations are naturally expressed in terms of  $q$ , and any attempt to extract a probability in terms of the planetary masses would have increased already lengthy calculations by an order of magnitude. As it is debatable whether mass or mass ratio is the more interpretable quantity, the small return is not worth the considerable extra effort. To determine a dependence of the detection probabilities on Galactic parameters, we must necessarily average the probabilities over distributions of quantities, such as lens mass, that remain inherently unknown and over other quantities such as source-lens impact parameter that are not *a priori* known. Details of the dependence of the detection probability on most of the parameters involved are shown as these averages are calculated. In this process we show that the  $S/N$  criterion leads to maximum averaged probabilities of detection that are comparable to or even greater than that obtained by Gould and Loeb for plausible assumptions of Galactic parameters, event geometries and observing telescopes. Perhaps more importantly, these probabilities remain robust as the parameters are varied within reasonable ranges. We should emphasize to the reader that the probability is not that of detecting a planet during any random event, but only the probability of detection if the lens has a planetary companion.

Hence, the success of any search program depends on the frequency of planetary occurrence, but null results will be meaningful in the sense that if the planets are there, they will be detected with reasonable probability.

An  $S/N$  criterion has been used previously to determine empirical planet detection probabilities for an individual event (Gaudi and Sackett, 2000; Albrow, *et al.* 2000a; Albrow *et al.* 2000b). A best fit single lens light curve for a point source-point lens model is determined from a given event data set by minimizing  $\chi_{PSP}^2$  with free parameters  $t_0, t_E, u_{min}, F_0, f_B$ . The time of minimum separation between source and lens is  $t_0$ ; the event time scale  $t_E = R_E/v_{\perp}$ , where  $v_{\perp}$  is the relative transverse velocity of source and lens projected onto the lens plane; the source-lens impact parameter is  $u_{min} = \gamma_{min}/\gamma_E$ , with  $\gamma_{min}$  being the minimum angular separation of source and lens during the event and  $\gamma_E = R_E/D_{OL}$ ; the unamplified flux density from the source is  $F_0$ ; and the ratio of the blended flux density from unresolved stars to the source flux density is  $f_B$ . To check if a binary lens gives a better fit to the data, one assumes a fixed planet-lens mass ratio  $q$ , a fixed projected planet separation  $b = r/R_E$ , and a projected source trajectory through the lens plane inclined at angle  $\alpha$  relative to the lens-planet line and again minimizes  $\chi^2$  with the same set of free parameters. A planet is assumed detected if  $\Delta\chi^2(q, x_p, \alpha) = \chi_{PSP}^2 - \chi^2(q, x_p, \alpha) > \Delta\chi_{thresh}^2 = 100$ , where the latter value is considered sufficiently large to be a secure better fit to the data (Gaudi and Sackett, 2000). To determine the efficiency of detecting a  $q, b$  planet for a particular event, the above process is repeated for a uniform distribution of  $0 \leq \alpha \leq 2\pi$ , and light curves which would have  $\Delta\chi^2 = \chi^2(q, x_p, \alpha) - \chi_{PSP}^2$  greater than some threshold would indicate that the planet would have been detected. The detection efficiency (probability)

$$\epsilon(x_p, q) = \frac{1}{2\pi} \int_0^{2\pi} \Theta[\Delta\chi^2(x_p, q, \alpha) - \Delta\chi_{thresh}^2] d\alpha \quad (2)$$

is the fraction of trajectories for which  $\chi^2(x_p, q, \alpha)$  exceeds the threshold value for detection for this  $(x_p, q)$ , where  $\Theta(x)$  is a step function. The probability in terms of the orbit semimajor axis in AU and planet mass  $m$  is estimated by assuming representative values of the lens mass and the lens and source distances.

This procedure confirms that planet detection during a microlensing event has a significant probability

ity for individual events. We show in Section 7 how  $\epsilon(x_p, q)$  can be averaged over the degenerate parameters in the Einstein ring radius weighted by the distribution of lenses and sources along the LOS and over the mass function (MF) yielding a probability of detection  $P'(a, q)$  applicable to that particular event with its determined source magnitude and normalized impact parameter. The Gaudi-Sackett procedure cannot be used to obtain the overall averages sought here for arbitrary events. Here we have no data sets on which to establish a  $\chi^2$  criterion, so the reference light curve will be that of the single lens without the planet, and the perturbations by the presence of a planet will be relative to this single lens curve. Since in the real world one has only best fit single lens light curves and best fit binary lens light curves for comparison, both of which tend to suppress any perturbations, our probabilities will be somewhat over estimated. This overestimate will be at least partially compensated by our procedure which tends to underestimate the probabilities.

We justify below the assumption that a planet will be detectable if the fractional perturbation of the light curve and hence the mean of a set of points during the perturbation exceeds  $2/(S/N)$  for the magnified source. Implicit in this assumption is that the perturbation be observed sufficiently long that enough photometric points can be obtained to establish the path of the photometric deviation with more than 99% confidence. In this sense, the  $S/N$  for the entire set of anomalous points will be  $\sqrt{\mathcal{N}}$  greater than that for an individual point, where  $\mathcal{N}$  is the number of photometric points during the perturbation. We argue below that  $\mathcal{N} = 20$  will establish a detection with greater than 99% confidence if the true mean of the set of perturbed points is displaced at least  $2/(S/N)$  from the unperturbed single lens light curve. Our neglect of the non-zero angular size of the source will limit  $q \geq 10^{-4}$ , where perturbation durations ( $2\sqrt{q}t_E$ ) will be a significant fraction of a day. So for almost all binary geometries where the planetary perturbation will exceed  $2/(S/N)$ , the duration of the perturbation will be sufficient to establish a reliable mean of the light curve during the perturbation—especially since the sampling frequency will most likely be drastically increased during the perturbation.

The  $S/N$  used as the detection criterion is developed in Section 2, where the  $S/N$  from photon statistics and sky noise is reduced by a constant factor to account for systematic and other unmodeled

noise and thereby approximate two independent empirical determinations of  $S/N$  for real systems. As we shall need a luminosity function (LF) to determine the fraction of the sources that are visible at any distance  $D_{OS}$ , we also introduce in this section the LF in  $I$ -band along with its adjustment for the source distance and extinction thereto. We have chosen the Holtzman *et al.* mass function (MF) for the lenses but the Zocalli *et al.* (2000) LF for the sources. Although Holtzman *et al.* (1998) determine an  $I$ -band LF for the Galactic bulge on the way to deriving their MF, it spans only about 9 magnitudes. But Zocalli *et al.* (2000) have obtained a deeper bulge LF in  $J$ -band for the lower main sequence and have supplemented their main sequence LF with the bulge giant LF obtained from Tiede *et al.* (1995) and Frogel and Whitford (1987) to obtain a more complete LF for the bulge that spans 15 magnitudes. The straight line segment representation of the main sequence part of the Holtzman *et al.*  $I$ -band LF has the same slope as the LF given in Section 2 within the uncertainties, so we keep the MF of Holtzman *et al.* (1998) that was derived from their LF, since programs incorporating it had been written earlier and since the MFs of several other studies also have an index of 1 in the M star region (*e.g.* Basu and Rana, 1992; Gould, Bahcall and Flynn, 1997 if unresolved binaries are accounted for (Gould, private communication, 1998)), but use the more complete  $I$ -band LF developed from the  $J$ -band LF of Zocalli *et al.* (2000) in Appendix A. Zocalli *et al.* (2000) derive a slightly steeper MF in the M star region than Holtzman *et al.* (1998) (index=1.3 vs 1). The change of the index from 1 to 1.3 in the M star region has only a small effect on the detection probability. We choose to illustrate the effect of increasing the MF index in the M star region by the relatively large index of 2.2.

We introduce the fundamental idea of the probability of detection based on an  $S/N$  criterion in Section 3. Here contours of the projected position of the planet onto the lens plane, within which the fractional perturbation of the single lens light curve exceeds  $2/(S/N)$  in magnitude, are shown to sweep out an area in the lens plane as the source passes by the lens at an impact parameter  $u_{min} = r_{min}/R_E$ . The extent of the the area grows with increasing  $q$ , with increasing  $S/N$ , and with decreasing  $u_{min}$ . We shall assume  $q = 0.001$  for most of the calculations, but we also show a completely averaged probability as a function of the planet semimajor axis for  $q = 0.0001$ .

(The  $S/N$  determined from Section 2 is a function of the  $I$ -band magnitude of the amplified source for a 2 meter telescope and 60 second integration times.) If the projected position of the planet is anywhere inside this area, the planet will cause a fractional perturbation of the single lens light curve exceeding  $2/(S/N)$  for a time of order  $2\sqrt{q}t_E$  sometime during the event and be detected (*e.g.* Gould and Loeb, 1992). The probability of detection is just the probability that the projected position of the planet is within the area swept out by the contours. (The amplification of the source for various configurations of the lens-planet binary system and the generation of contours of constant perturbation of the single lens light curve used extensively in this section are developed in Appendix B.) Also illustrated in this section is the reason for the unit probability of detection in the annular “lensing zone” region straddling  $R_E$  for high amplification events (Griest and Safizadeh, 1998.)

The probability of the projected planet position is developed in Section 4 and Appendix C. To average over unknown orbital inclination and planet orbital longitude, a planet is assumed to be uniformly distributed over a sphere of radius  $a$ , and the probability  $F(r)$  that the projected separation of the planet from the lensing star is between  $r$  and  $a$  is determined therefrom (Gould and Loeb, 1992).  $F(r)$  is expressed in terms of  $x_p = r/R_E$  and  $a/R_E$ , as this is the normalization under which the microlensing amplification is expressed. Then  $F(r) \rightarrow F(x_p, a, \zeta, z, M)$ . The explicit display of  $M$ ,  $z$  and  $\zeta$  in  $F(x_p, a, \zeta, z, M)$  follows from  $R_E$  (Eq. (1)), and the degeneracy of these variables in any microlensing event makes necessary an average over  $z$  from observer to source weighted by the distribution of lenses along the LOS and an average over  $M$  weighted by the MF to yield  $F(x_p, a, \zeta)$  (Appendix C). The average over  $\zeta$  weighted by the distribution of sources along the LOS must follow an average of the probability over the LF.  $F(x_p, a, \zeta)$  is the probability of finding the projected position of the planet between  $x_p = r/R_E$  and  $a/R_E$  averaged over the lens MF and the distribution of lenses along the LOS from the observer to the source, and  $-dF(x_p, a, \zeta)/dx_p$  is the probability density. The Zhao (1996) bulge model is combined with the Bahcall-Soneira (1980) disk model to determine the spatial distribution of lenses. We have already pointed out our choice of the Holtzman *et al* (1998) MF above. The probability of detection is now initially developed for fixed  $a$  and  $\zeta$  for a par-

ticular source  $I$ -band apparent magnitude. Eleven values  $0.6 \leq a \leq 10.0$  are carried through the remaining steps to obtain a final averaged probability as a function of  $a$ .

In Section 5, for  $q = 0.001$  and given  $I$ -band magnitude of the source,  $a$  and  $u_{min}$ , we determine the probability  $P(a, \zeta, I, u_{min})$  of detecting a planet of semimajor axis  $a$ , when the normalized source distance is  $\zeta$ , the source magnitude is  $I$  and the source-lens impact parameter is  $u_{min}$ . This is accomplished by determining the boundaries of the area swept out in the lens plane by the contours of the  $2/(S/N)$  fractional perturbation of the single-lens light curve and integrating the probability density of the planet projection over the area, where the latter simply uses differences in  $F(x_p, a, \zeta)$  for two pairs of values of  $x_p$  defining the boundaries of the area at stepped intervals along the source trajectory.  $P(a, \zeta, I, u_{min})$  is determined for a distribution of impact parameters  $0 < u_{min} < 1$ , and the results averaged over  $u_{min}$  to yield  $P(a, \zeta, I)$ , which is the probability of detection for the given  $q = 0.001$ , semimajor axis, source distance and source  $I$ -band magnitude averaged over the distribution of planetary orbital inclinations and phase, over the distribution of lenses along the LOS, over the MF, and over the distribution of  $u_{min}$ . These probabilities are determined for a grid of values of  $\zeta$ ,  $I$ . It is also shown here how the peak of the detection probability moves toward smaller values of  $a$  as the source moves closer to the observer, which reflects its following the mean value of  $R_E$ .

For each  $\zeta$  the span of likely values of  $I$  is determined according to the LF as modified by the distance to and extinction of the source with  $I < 21$  assumed to be the largest magnitude for which useful high precision, high time resolution photometry could be carried out. [For data sets for which image differencing (*e.g.*, Alcock *et al.* 2000) or other techniques have not been employed to pick up many of the events with fainter sources, the number of usable faint sources will be reduced from that implied by the real LF with  $I < 21$ . Reducing the fraction of sources with low luminosities would actually increase the averaged probabilities, since the brighter stars will have a higher S/N. (See Fig. 11.)] The  $P(a, \zeta, I)$  is then averaged over  $I_{min} < I < 21$  weighted by the LF for each  $\zeta$  to obtain  $P(a, \zeta)$  for each  $\zeta$ .  $I_{min}$  corresponds to the brightest star kept in the LF; it decreases as the source distance  $\zeta$  is decreased or the extinction is reduced. Illustrations of the dependence of the detec-

tion probability on source distance and source magnitude for averages over the LF at each source distance are also given in Section 5. The dependence of  $I$  on  $\zeta$  is why we delayed averaging over the latter until the average over the LF could be completed.

For  $0.1 < \zeta < 1.2$ ,  $P(a, \zeta)$  is averaged over the distribution of *visible* sources along the line of sight in Section 6 to yield  $P(a)$ , where “visible” means  $I < 21$  as discussed above.  $P(a)$  is the probability of detecting a planetary companion of a lens with  $q = 0.001$  and semimajor axis  $a$  (for 11 values of  $a$ ) during a microlensing event averaged over all of the Galactic and geometric parameters. The same galactic model used for the distribution of lenses is used for the distribution of sources. The lower limit on  $\zeta > 0$  is chosen to avoid a singularity in the expressions, where a source at  $\zeta < 0.1$  is extremely unlikely in any case. The upper limit is chosen 1.2 since extinction and blending will make the number of sources that are useably visible negligibly small at larger  $\zeta$ . It is shown here that for a LOS toward Baade’s window, the peak probability of detection exceeds 10% for  $a$  near the mean value of  $R_E$  of almost 2 AU, if  $u_{min}$  is distributed uniformly, but it exceeds 20% for a distribution determined by the observational efficiency for the events, which has a higher proportion of small  $u_{min}$ .

To clarify the series of averages, we write an equation for  $P(a)$  that includes all of the averaging operations except the initial one over the planetary orbital inclination and phase, where the latter is accomplished simply by the assumption of uniform distribution over a sphere of radius  $a$ .

$$\begin{aligned}
P(a) = & \int_{0.1}^{1.2} n'_s(\zeta) d\zeta \int_{I_{min}}^{21} LF(I, \zeta, A) dI \\
& \times \frac{1}{k} \sum_{i=1}^k \iint_{S(I, u_{min}^i)} dS \left( -\frac{d}{dx_p} \right) \\
& \times \int_0^\zeta \int_{M_{min}}^{M_{max}} n'_L(z, M) \Theta[f(x_p, a, \zeta, z, M)] \\
& \times F(x_p, a, \zeta, z, M) dz dM, \tag{3}
\end{aligned}$$

where  $\Theta[f(x_p, a, \zeta, z, M)]$  is a step function whose argument  $> 0$  [given in Eq. (C1)] is a condition for the reality of  $F(x_p, a, \zeta, z, M)$ ;  $n'_L(z, M)$  is the fraction of lenses in volume  $z^2 dz \Delta\Omega$  and in mass range  $dM$  of those along the LOS to the source with  $\Delta\Omega$  being a representative solid angle in the field;  $S(u_{min}^i, I)$  is the area in the lens plane corresponding to the particular

$u_{min}^i$  and source  $I$ -band magnitude within which a planet would cause a perturbation of the light curve exceeding  $2/(S/N)$ . The double integral on the far right is  $F(x_p, a, \zeta)$  so  $-dF(x_p, a, \zeta)/dx_p$  is the probability density, which is integrated over the area in the next integral to the left to yield  $P(a, \zeta, I, u_{min}^i)$ . The sum of  $P(a, \zeta, I, u_{min}^i)$  over the  $k$  values of  $u_{min}$  divided by  $k$  gives the average over the impact parameters to yield  $P(a, \zeta, I)$ .  $LF(I, \zeta, A)$  is the fraction of sources per unit  $I$  magnitude adjusted for distance and extinction  $A$ . This integral over the LF yields  $P(a, \zeta)$ . Finally,  $n'_s(\zeta)$  is the fraction of *visible* sources of those along the line of sight, and the integral over  $\zeta$  yields  $P(a)$ .

Section 7 shows how the detection probability changes as various parameters are changed. It decreases as the extinction is increased or if the detection criterion is increased from  $2/(S/N)$  to  $3/(S/N)$ . Changing the LOS changes the distribution of the probability over the values of  $a$  by changing the mean  $R_E$ . Here we show how increasing the fraction of M-type stars in the MF drives the peak in the probability to smaller values of  $a$ , while decreasing the probability for large  $a$  and increasing the probability for small  $a$ . We have already pointed out above the conversion of the model independent  $\epsilon(x_p, q)$  to the model dependent  $P'(a, q)$  at the end of Section 7.

The properties of the averaged planetary detection probability are summarized in Section 8 where it is also shown how the detection probability, averaged over everything except the LF, varies with the source magnitude. Also shown here is the detection probability as a function of the planetary semimajor axis for a particular event, where the source magnitude and the impact parameter are assumed known. A discussion follows in Section 9, where the robustness of relatively large detection probabilities over a wide range of planetary semimajor axes to variations in the various parameters is emphasized, while the dependencies on assumptions and other caveats and neglected processes are pointed out. The unique aspects of a microlensing search for planets and the robustness of the probabilities of detection for all plausible variations in Galactic parameters are additional justifications for the continued pursuit of ground based microlensing searches for planets in spite of the exponentially growing success of radial velocity searches and proposed space based microlensing searches.

## 2. Signal to noise ratio.

The part of  $S/N$  appropriate to photometry of a star that depends on just photon statistics and sky noise can be written (up to the factor 1/4 in parentheses)

$$\begin{aligned} \frac{S}{N} &= \frac{\phi_{star} \sqrt{A_T E t}}{\sqrt{A_s \Phi_{sky} + \phi_{star}}} \left( \times \frac{1}{4} \right) \\ &= \frac{314 \times 10^{-0.4I} D \sqrt{t}}{\sqrt{2.23 \times 10^{-8} + 10^{-0.4I}}} \left( \times \frac{1}{4} \right), \quad (4) \end{aligned}$$

where  $\phi_{star}$  (photons/cm<sup>2</sup>sec) is the photon flux density from the source star,  $A_T = \pi D^2/4$  (cm<sup>2</sup>) is the telescope aperture area ( $D$  = aperture diameter),  $E$  is the overall efficiency of the system,  $\Phi_{sky}$  (mag/arcsec<sup>2</sup> → photons/(cm<sup>2</sup>sec arcsec<sup>2</sup>)) is the surface brightness of the sky,  $A_s = \pi s^2/4$  (arcsec<sup>2</sup>) is the seeing disk ( $s$  = seeing defined as the FWHM of the point spread function) and  $t$  (sec) is the integration time. From the lines just preceding Eq. (A7), the  $I$ -band flux density from Vega is  $1.56 \times 10^{-6}$  erg cm<sup>-2</sup>sec<sup>-1</sup> leading to  $\phi_{star} = 6.28 \times 10^5 10^{-0.4I}$  photons cm<sup>-2</sup>sec<sup>-1</sup> for magnitude  $I$  with a square profile for the  $I$ -band filter  $0.13 \mu\text{m}$  wide at  $0.8 \mu\text{m}$  ( $I_{Vega} = 0$ ). The clear night sky brightness at Cerro Tololo Interamerican Observatory in  $I$ -band ranges from 19.2 to 19.9 magnitudes arcsec<sup>-2</sup> (Walker, 1987) from full to new moon. We choose an average sky brightness of 19.6 magnitudes arcsec<sup>-2</sup>,  $s = 1.4$  arcsec and  $E = 0.2$  to yield the final form of Eq. (4) without the factor (1/4).

Eq. (4) without the factor 1/4 does not yield values of  $S/N$  close to those empirically determined because of instrument and systematic noise, reduced flux from sky absorption and effects of other varying observing conditions that have been omitted. To account in an approximate way for these omitted quantities, we reduce the coefficient of the  $S/N$  from photon statistics and sky noise until  $S/N$  matches the empirical data of Albrow *et al.*, (1998). For  $D = 91$  cm and  $t = 300$  sec, Albrow *et al.* obtain 1%, 2%, 7% photometry for  $I = 15, 17, 19$  respectively. For  $I = 19$ , substitution of these values of  $D$  and  $t$  into Eq. (4) yields  $S/N = 57$  instead of a little over 14 for the 7% photometry found by Albrow *et al.* The empirical datum is matched if we multiply Eq. (4) by the indicated factor of (1/4). Table 1 compares the  $S/N$  determined by Eq. (4) with the empirical values of Albrow *et al.* for the remaining two magnitudes and for empirical values for a 76 cm telescope at Lick Observatory (W.

Li and A. Filippenko, Private communication, 2000). The Albrow *et al.* data are nearly matched for all the magnitudes, whereas the Lick data are reproduced for the brighter magnitudes, but less well for the magnitudes near the limiting value for the telescope. Eq. (4) as modified is thus a good approximation at least to the Albrow *et al.* data, and reproduces much of the Lick data. These comparisons with empirical data encourage the use of Eq. (4) for our purposes here. In determining  $S/N$  to be used in finding the probability of detecting a planetary companion of a lens during an event, we shall assume  $D = 200$  cm and  $t = 60$  sec, except we shorten the integration time for bright sources to keep  $S/N < 200$ . Systematic effects would probably soon dominate photon statistics for the brighter sources, so  $S/N$  would not be improved by longer integrations.

I mag	Albrow <i>et al.</i>	Lick
	D=91 cm t=300 sec s=1.4 as	D=76 cm t=300 sec s=2.24 as
15	100, <b>122</b>	> 80, <b>100</b>
17	50, <b>46</b>	35, <b>35</b>
18.5		6, <b>13</b>
19	14, <b>14</b>	2-3, <b>9</b>

Table 1: Comparison of empirical determinations of  $S/N$  with those determined by Eq: (4) including the factor 1/4. The calculated values of  $S/N$  are in bold-face type next to the empirical values.

Subjective impressions of examples of precision photometry in the literature, (*e.g.* Charbonneau *et al.* 2000), suggest that a  $2\sigma$  perturbation of a single lens light curve should be easily discerned with a sufficient number of data points, where  $\sigma = 1/(S/N)$  is the rms fractional deviation of points about the best fit curve (*e.g.*,  $\sigma = .01$  is 1% photometry). What is “sufficient” is also subjective, but we can quantify this in terms of confidence. We consider a microlensing event of duration 30 days ( $2t_E$ ) perturbed by a planet with  $q = 0.0001$ , where the expected duration of the perturbation is  $\sim 2\sqrt{q}t_E = 0.3$  days (*e.g.*, Peale, 1997). As an example, we assume a worst case true perturbation of the single lens light curve remains at the minimum  $2/(S/N)$  for the entire 0.3 days, where  $S/N$  is that for a single observation of the amplified brightness of the source, which will not change significantly during the short time of the perturbation. This example perturbation is unlike a true



planetary perturbation, but its simplicity and minimal nature will illustrate the viability of our detection criterion adequately. We want to find an estimate of the number of data points necessary to detect such a perturbation coupled with a measure of the confidence in the detection.

In Fig. 1, we show a segment of a microlensing light curve with  $u_{min} = 0.2$  for a source magnitude  $I = 20$  with this minimum assumed perturbation that occurs about 4.5 days after the time of the peak amplification. The solid bold line is the true amplification of the source, and the dotted curves span the true unperturbed light curve by a fraction  $\pm 2/(S/N)$ .  $S/N$  as determined by Eq. (4) has a relatively poor value of about 15 at the region of the curve where the perturbation occurs. The simulated data points are normally distributed with  $\sigma$  for the fractional deviation equal to the local value of  $1/(S/N)$ . The sampling frequency is once per hour outside the perturbation region, but it is increased to once every 5 minutes during the perturbation with the same conditions (integration time, telescope, *etc.*) determining  $S/N$  as for the remaining part of the light curve. The two short lines closest to and on either side of the bold line are least squares fits to a straight line for the 86 simulated data points and to the same set with opposite signed, equally probable deviations. The uncertainty  $\sigma_{det}$  in the mean position of the normalized data points during the perturbation is  $\sigma/\sqrt{N} = 1/(\sqrt{86}S/N)$ , which is a measure of the uncertainty in the detection. The effective  $S/N$  for the detection is more than 9 times that for each individual point and the detection is essentially certain. That is, with 99% confidence, the true amplification is within  $3\sigma_{det} = 1/(3S/N)$  of the measured mean represented by the midpoint of the either of the two short lines segments closest to the true light curve during the perturbation. The uncertainty is small compared with the magnitude of the fractional perturbation of  $2/(S/N)$ .

The other two small line segments separated further from the true light curve correspond to least squares fits to only 20 points taken during the perturbation, which is a sampling frequency about 3 times that for the other parts of the light curve. Here  $\sigma_{det} = 1/(\sqrt{20}S/N)$  and there is 99% confidence that the true amplification falls within about  $2/(3S/N)$  of the midpoint of either line. This is still sufficiently less than the  $2/(S/N)$  perturbation that a detection would be secure. There is a necessary cushion here, because the entire light curve will only be a best fit

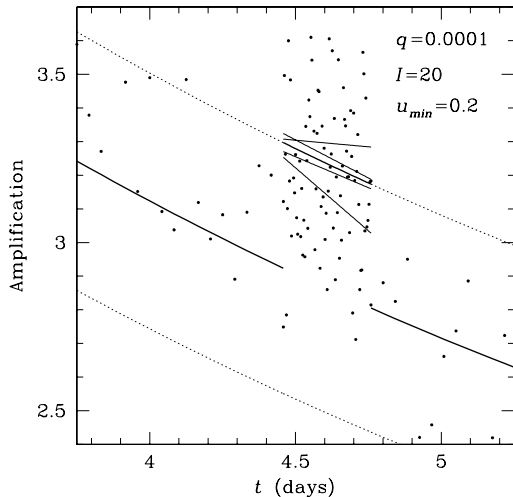


Fig. 1.— Segment of a microlensing light curve for  $I = 20$ ,  $u_{min} = 0.2$ , and  $q = 0.0001$ , where the duration of the planetary perturbation is  $2t_E\sqrt{q} = 7.2$  hours for an event duration of 30 days. The bold lines represent the true amplification and the dotted lines are displaced by a fraction of  $\pm 2/(S/N)$  from the true amplification. The simulated points are gaussian distributed with  $\sigma = 1/(S/N)$ . The two short thinner lines on either side of and closest to the bold line during the perturbation are least squares fits to the set simulated data points and to a set where each deviation is given the opposite sign. The second set of lines further separated from the true amplification during the perturbation are least square fits to only 20 data points.

model of all of the points, and the perturbation will be suppressed somewhat during the fit. If we assume a planetary perturbation of the single lens light curve that exceeds  $2/(S/N)$  can be detected with 20 consecutive data points during the perturbation, confidence in the detection would exceed 99% even for the minimum perturbation. A detection criterion can then be defined as a fractional perturbation of the single lens light curve that exceeds  $2/(S/N)$  for at least 20 consecutive data points. Sufficient duration of a perturbation to satisfy this criterion will obtain for almost all of the events considered in determining the probabilities for reasonable sampling rates with the applicable values of  $q$ , and duration will not appear

explicitly in the calculations to follow. In this sense, duration is really not part of the detection criterion used in the calculations, but the constraint of “20 consecutive data points” is understood to be satisfied for nearly all detectable events. Note that for the minimum fractional perturbation of  $2/(S/N)$ , some part of the perturbation will probably have passed before a higher sampling frequency and perhaps longer integration times were effected to more closely map the perturbed part of the light curve. Hence, a detection does not necessarily imply sufficient definition of the light curve to constrain  $q$  adequately. In addition, the poorer definition of the slope of the best fit curves when only 20 data points are available illustrates the necessity of very frequent sampling if one hopes to characterize the planet with any certainty. It is certainly clear from Fig. 1 that an  $S/N$  considerably better than 15 is desirable for characterizing the planet, but the smaller values do not preclude detecting a  $2/(S/N)$  perturbation with 20 data points.

The  $S/N$  used to establish the criterion for detecting a planetary companion during a microlensing event depends of course on the apparent brightness of the source star. The distribution of the apparent brightness of the source stars at a particular distance are determined from the following LF.

$$\begin{aligned}
 f_L(I_8) &= 1.470 \times 10^{-9} e^{0.930 I_8} & 10.5 \leq I_8 \leq 17 \\
 &= 2.575 \times 10^{-8} e^{0.762 I_8} & 17 \leq I_8 \leq 18.5 \\
 &= 1.316 \times 10^{-4} e^{0.300 I_8} & 18.5 \leq I_8 \leq 26,
 \end{aligned}
 \tag{A5}$$

which represents the fraction of the sources per unit  $I$  magnitude for bulge stars at a distance of 8 kpc.  $I_8$  is the  $I$  magnitude at that distance. This  $I$ -band LF is constructed from the  $J$ -band LF of Zoccali *et al.* (1999) in Appendix A, where the  $I$ -band is chosen as the most likely bandpass that will be used in any dedicated planet search from the ground. In Eqs. (A5),  $10.5 < I_8 < 17$  corresponds to giant stars and  $18.5 < I_8 < 26$  to main sequence stars below the turnoff with the second of Eqs. (A5) bridging the gap between the two distributions. The same luminosity function will be assumed to apply to the disk as well as the bulge, although there will be fewer giants among the disk stars. Most of the sources will be in the bulge in any case, and changes induced in the probability calculations by a more refined LF are negligibly small.

For particular LOS,  $\zeta$ ,  $q$ ,  $a$  and MF of the lenses,

the probability of detection is calculated for a few tens of values of the impact parameter ( $0 < u_{min} \lesssim 1$ ) and the probabilities averaged over the impact parameter distribution. This is done for approximately 10 different apparent magnitudes in the range  $I_{min} < I < 21$ . The maximum value of  $I = 21$  is chosen as the dimmest star that can be usefully monitored in a ground based search for planetary perturbations, whereas  $I_{min}$  is determined by the brightest star in the LF translated to distance  $\zeta$  and increased by the extinction to that distance. The extinction is handled by assuming that the measured extinction to 8 kpc along the particular LOS is uniformly distributed from the observer to 8 kpc. The transformation of the LF of Eq. (A5) to one for the apparent magnitude at distance  $\zeta \neq 1$  is effected by substituting

$$I_8 = I_{app} - A_{I_8} \zeta - 5 \log \zeta \tag{5}$$

into the LF, where  $A_{I_8}$  is the extinction to 8 kpc. Details are given in Appendix A.

### 3. Probability of detection

The basic idea behind the detection probability is due to Gould and Loeb (1992), although we use an  $S/N$  criterion for detection instead of a fixed percentage perturbation of the microlensing light curve. Fig. 2 shows loci of equal amplification for the positions of a planet projected onto the lens plane with planet-star mass ratio  $q = 0.001$ . The amplification of the source is  $A = [1 \pm 2/(S/N)]A_0$  if the planet is on a contour, where  $A_0$  is the unperturbed amplification of the source if the planet were not there. A fractional perturbation of  $2/(S/N)$  is assumed detectable with  $(S/N)$  being that appropriate to the instantaneous brightness of the amplified source. Inside the loci the perturbation will exceed  $2/(S/N)$  in magnitude. The method of estimating  $S/N$  for a given source magnitude is shown in Section 2 above.

As the source passes by the lens from left to right in Fig. 2, the contours sweep across the lens plane—waxing and waning as the source gets closer to or further from the lens and as  $S/N$  varies with the instantaneous value of  $A_0$ . The large curves trace the extremes of the equal amplification loci during the traverse of the source across the Einstein ring, and a planet would be detected at some time during the event if its projected position were anywhere within either pair of the large curves. We adopt the probability of detecting the planet during the event as the

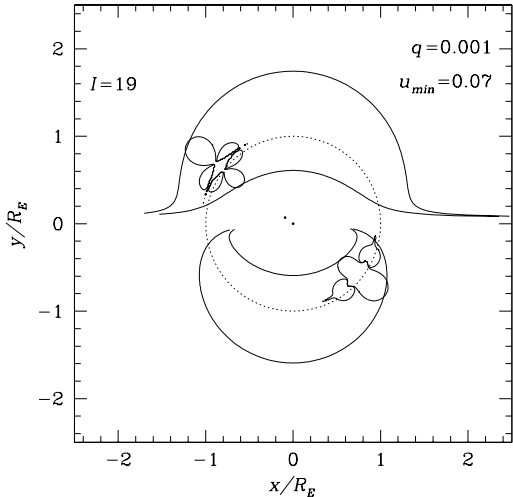


Fig. 2.— Sweep of small contours of  $\pm 2/(S/N)$  fractional perturbation of light curve across the lens plane. The large curves are traces of the extremes of the contours during the event, and they define the area within which a planet would be detected if it happened to be there. The source magnitude is  $I=19$ . The diagram is centered on the lens with the position of the source corresponding to the contours displaced a small distance into the second quadrant. The dotted circle is the Einstein ring. At the source location shown,  $2/(S/N) = 0.0366$ , whereas at closest approach  $2/(S/N) = 0.0283$ . The source moves horizontally across the diagram.

probability that its projected position is within the area contained by the large curves. This area expands and the probability of detection is correspondingly higher as the source brightness is increased thereby increasing  $S/N$  and as the impact parameter of the source-lens encounter is reduced. The contours shrink or expand approximately as  $\sqrt{q}$ , and the area between the trace curves and probability of detection are changed approximately by the same factor.

Fig. 3 shows how the area is increased with source brightness. The effect on the probability of this change in area is shown in Fig. 4, where the detection probability is increased for brighter stars for all  $u_{min}$ . Fig. 4 also illustrates the increased probability of detection for smaller  $u_{min}$ . The impact parameter of 0.07 in Fig. 2 is reduced to 0.005 in Fig. 5,

which shows the expanded loci of minimum perturbation for detection and the expanded curves tracing the extremes of these loci. One notices first in Fig. 5 that the loci extend beyond the traces of their extremes along their symmetry axes (the source-lens line), so that the probabilities are slightly underestimated by our adopted scheme. That is, a planet would still be detected if it were slightly outside the curves defining the traces of the extremes of the loci contours. However, this effect is most pronounced for the smallest impact parameters where it makes at most a few percent difference in the calculated probability, and we average these probabilities over the distribution of impact parameters, which further reduces the relative contribution of this extra probability for small impact parameters. Notice next that the contours within which the planet would be detected completely encompass the region around the Einstein ring radius for small impact parameters. This illustrates the result of Griest and Safizadeh (1998) who found unit probability of planet detection for high amplification events if the projected position of the planet were anywhere within a region spanning the Einstein ring radius.

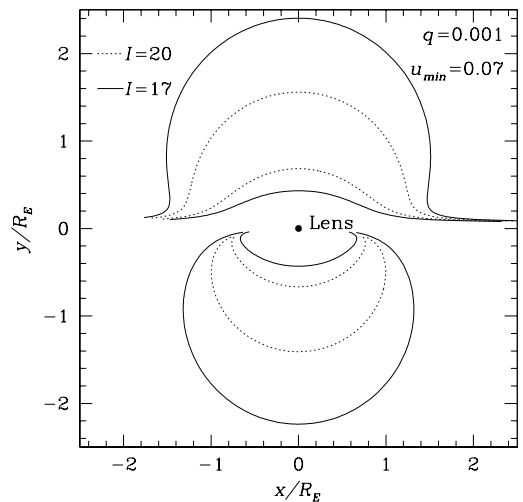


Fig. 3.— Traces of the extremes of the contours of  $\pm 2/(S/N)$  fractional perturbation of the light curve for  $q = 0.001$ ,  $u_{min} = 0.07$  and two stellar  $I$ -magnitudes. The area inside the curves and the probability of detection is higher for brighter stars.

The amplification of a source by a binary star-planet lens is determined in Appendix B with the analysis in the complex plane by Witt (1990). The procedures for determining the contours of equal amplification and for determining the extremes of these contours—used in Figs. 2, 3 and 5—are also outlined in this appendix.

#### 4. Probability distribution of the planet in the lens plane.

The time average separation of a planet from its primary is  $a(1 + e^2/2)$ , where  $a$  and  $e$  are the semi-major axis and eccentricity of the orbit. So we can account for the random orbit orientation and random phase by assuming that the instantaneous position of a planet is uniformly distributed over the surface of a sphere of this radius. However, we drop the  $e^2$  and assume the sphere has radius  $a$ , where it is understood that this “semimajor axis” is augmented by some assumed mean orbital eccentricity to represent an averaged separation. The cumulative probability that a planet with this distribution will have a position projected onto the lens plane between  $r \leq a$  and  $a$  is (Gould and Loeb, 1992)

$$F(r) = \sqrt{1 - \frac{r^2}{a^2}},$$

or between  $x_p = r/R_E$  and  $a/R_E$ ,

$$\begin{aligned} F(x_p, a, \zeta, z, M) &= \sqrt{1 - R_E^2 \frac{x_p^2}{a^2}} \\ &= \sqrt{1 - K \frac{M}{a^2} \frac{z(\zeta - z)}{\zeta} x_p^2}, \end{aligned} \quad (6)$$

where  $K = 4GM_\odot D_8 / (c^2 a_\oplus^2) = 65.1279$  with  $G$  = the gravitational constant,  $M_\odot$  = the solar mass,  $a_\oplus = 1$  AU,  $M$  is the lens mass in units of  $M_\odot$ , and  $a$  is now measured in AU in the last line.

We wish to determine a planet detection probability during a microlensing event in terms of a criterion based on a representative  $S/N$  of the signal. The latter depends on the apparent magnitude of the source, which in turn depends on  $\zeta$  for the given luminosity function. We therefore average the cumulative probability in Eq. (6) over the distribution of the lenses from the observer to a particular source distance  $\zeta$  and simultaneously over the MF of the lenses, since the lens mass  $M$  is embedded in the definition of  $R_E$  (Eq. (1)). The probability of detection of a planet

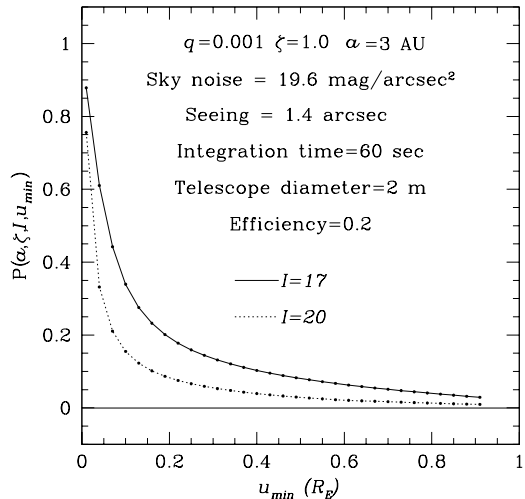


Fig. 4.— Detection probability for  $q = 0.001$ ,  $\zeta = 1.0$ ,  $a = 3$  AU as a function of the impact parameter for two different source brightnesses. The probability increases as  $u_{min}$  is reduced, and it is increased for all impact parameters for the brighter star.

of given  $q$  (averaged over the lens density distribution and MF about a star lensing a source of given  $I$  magnitude at given distance  $\zeta$ ) can then be averaged over the apparent brightness distribution from the LF as adjusted for that particular distance. After the probabilities are averaged over the MF, lens spatial density distribution and LF, they will then be averaged over the distribution of *visible* sources along the particular line of sight—all this as a function of the semimajor axis of the planetary orbit in AU. But first we must average  $F(x_p, a, \zeta, z, M)$  over the lens distribution between observer and source and over the MF.

The details of this averaging process are given in Appendix C. In the average represented by Eq. (C1),  $a$  and  $\zeta$  are fixed, and the average is performed as a function of  $x_p$ . The Holtzman *et al.* (1998) MF, which we represent as being  $\propto M^{-1}$  for  $0.08 \leq M \leq 0.7M_\odot$  and  $\propto M^{-2.2}$  for  $0.7 \leq M \leq 2M_\odot$ , is used in the averaging. The lens distribution is determined by the triaxial Galactic bulge model of Zhao (1996) combined with the double exponential disk model of Bahcall and Soneira (1980).

Fig. 6 shows the averaged cumulative probability  $F(x_p, a, \zeta)$  of the projected separation of the planet

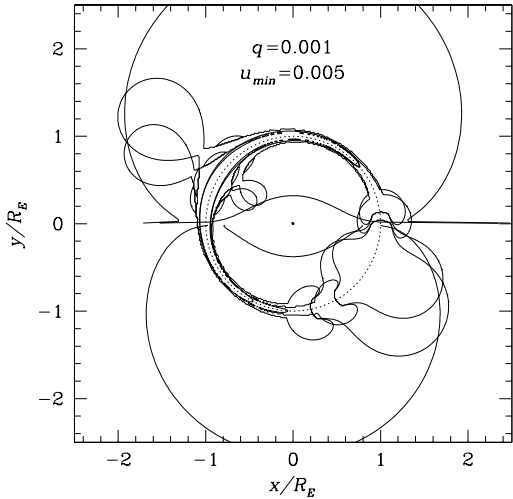


Fig. 5.— The contours defining a  $2/(S/N)$  perturbation of the light curve grow and the area inside large curves that trace the contour extremes along the source-lens line is increased as is the probability for detection for smaller impact parameters  $u_{min}$ . The area enclosed by the contours that is beyond the traces of the extremes means we underestimate the true probability of detection by a few percent for the smallest impact parameters. Here the fractional perturbation is fixed at 0.1.

from its star for several values of the orbit semimajor axis  $a$  for the particular choice of a LOS toward Baade’s window  $(\ell, b) = (1^\circ, -4^\circ)$  ( $\ell, b$  are Galactic longitude and latitude respectively) and for a source distance of 8 kpc ( $\zeta = 1$ ). The Holtzman *et al.* (1998) MF is adopted for both disk and bulge stars. Of course the cumulative probability is unity for  $x_p = 0$ , since it is certain that the projected position of the planet will be somewhere between 0 and  $a$ . The only contributions to  $F(x_p, a, \zeta)$  come from those lenses along the LOS where  $R_E < a/x_p$  (Appendix C). For small  $a$ , the number of lenses whose  $R_E$  values qualify plummets rapidly as  $x_p$  increases. Increasingly small  $M$  with  $z$  either very small or very near  $\zeta$  are required until there are no lenses at all along the LOS that satisfy the condition.  $F(x_p, a, \zeta)$  in Fig. 6 correspondingly decreases most rapidly toward zero when  $x_p$  increases for small  $a$  and less rapidly for larger  $a$ .

Useful in understanding Fig. 6, Fig. 7 shows the

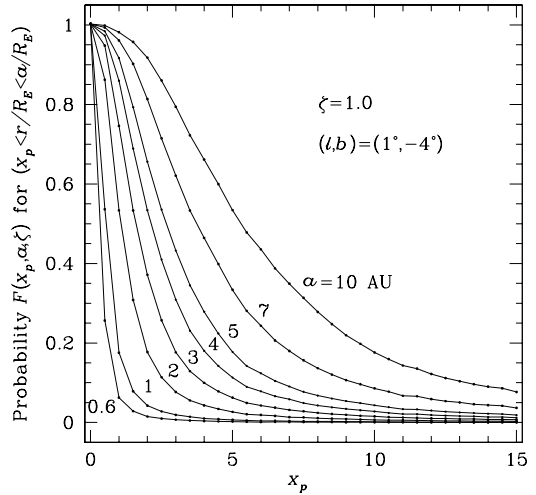


Fig. 6.— Cumulative probability  $F(x_p, a, \zeta)$  that the projected position of the planet lies between  $x_p$  and  $a/R_E$  for several values of semimajor axes  $a$  for a fixed source distance  $\zeta = 1$ . The probability is averaged over the line of sight distribution of lenses according to the Zhao bulge model and the Bahcall and Soneira disk model, and over the Holtzman *et al.* mass function.

Einstein ring radius averaged along the LOS to distance  $\zeta$  according to

$$\langle R_E \rangle = (8.07 \text{ AU}) \times \frac{\int_{M_{min}}^{M_{max}} \int_0^\zeta \sqrt{\frac{Mz(\zeta-z)}{\zeta}} z^2 \frac{dn_L(M, z)}{dM} dz dM}{\int_{M_{min}}^{M_{max}} \int_0^\zeta z^2 \frac{dn_L(M, z)}{dM} dz dM}, \quad (7)$$

where  $dn(M, z)/dM$  (given in Appendix C) is the number density of lenses per unit mass interval at position  $z \leq \zeta$  along the LOS. The integrals are evaluated with a Monte Carlo technique (Press *et al.* 1986).  $\langle R_E \rangle$  is shown for two MFs in Fig. 7, but concentrate on the one for the Holtzman *et al.* mass function for now. The relatively small value of  $\langle R_E \rangle$  for  $\zeta = 1$  results from the facts that the MF is dominated by M stars with small  $R_E$  and that  $R_E$  decreases as the lens approaches the source at  $\zeta = 1$  where the number density is highest. The curve for the modified Holtzman *et al.* MF ( $\propto M^{-2.2}$  in Fig. 7) will be

used later to illustrate the effect of changing the MF on the detection probability. The probability density

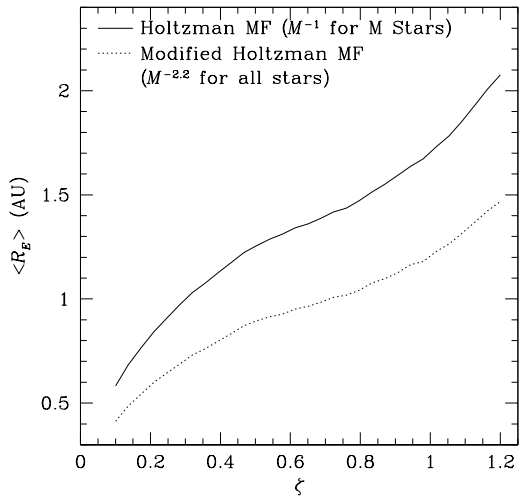


Fig. 7.— The Einstein ring radius averaged over the lens density distribution along the line of sight toward Baade’s window  $(\ell, b) = (1^\circ, -4^\circ)$  and over the indicated mass functions for the Zhao (1996) bulge and Bahcall-Soneira (1980) disk models.

of the planet separation is the negative derivative of these curves so the planet has the highest probability of being found at a value of  $x_p$  where the slopes are steepest. The curves approach zero slope more rapidly for the smaller semimajor axes, since it is less likely to find a close planet much outside the Einstein ring radius for the given MF. Similarly, the planet is more likely to have a large value of  $x_p$  if the semimajor axis is larger, so the value of  $x_p$  where the slope is steepest for a given  $a$  increases with  $a$ . The magnitudes of the slopes decrease as  $a$  increases since the probability density is spread over a greater area and must be thereby smaller. The probability density of the projected position is sharply peaked near  $r = a$  (Gould and Loeb, 1992). This is understood intuitively since the planet spends a higher fraction of the time near the extremes of its projected orbit as it travels toward or away from the observer. Or from the uniform distribution over the surface of the sphere, a large area of the sphere is covered by small changes in the LOS near the extreme. The steepest slope for, say,  $a = 2$  AU in Fig. 6 occurs near  $x_p = 1$ , which reflects

the fact that the average  $R_E$  over the LOS to  $\zeta = 1$  is about 1.7 AU. (That is,  $x_p = r/R_E$  and  $r$  prefers to be near  $a$  because of the peak at  $a$  in the probability density.) The steepest slope for  $a = 10$  AU occurs near  $x_p = 5$  or 6, which is again the planet preferring to be at an extreme separation with  $\langle R_E \rangle \approx 1.7$  AU.

Fig. 8 shows the same cumulative probability distribution as Fig. 6, but now  $a$  is fixed at 3 AU and the distance to the source is varied. Again contributions to  $F(x_p, a, \zeta)$  come only from those lenses with  $R_E < a/x_p$ . From Fig. 7 we see that  $\langle R_E \rangle$  is large for large  $\zeta$ , so as  $x_p$  increases, the number of lenses along the LOS contributing to  $F(x_p, a, \zeta)$  decreases most rapidly for large  $\zeta$ . That is, if  $\langle R_E \rangle$  is large, the number of lenses with sufficiently small  $R_E$  to contribute to  $F(x_p, a, \zeta)$  plummets most rapidly as  $x_p$  increases for large  $\zeta$ , and the number decreases less rapidly for smaller  $\zeta$  when  $x_p$  increases. These trends are evident in Fig. 8.

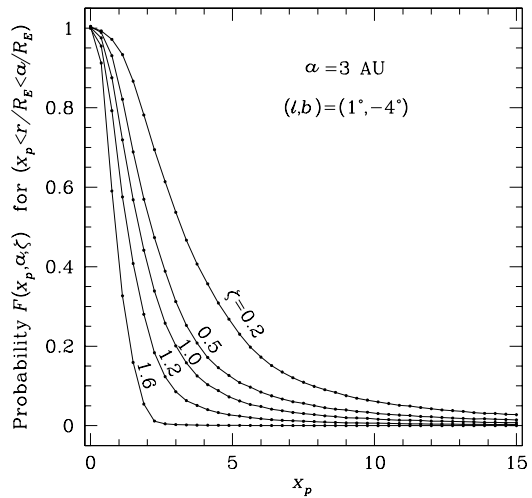


Fig. 8.— Same as Fig. 6 except the cumulative probability is given for several values of source distance  $\zeta$  for fixed semimajor axis  $a = 3$  AU.

Since the probability density of the projected planet position peaks near  $r = a$ , the planet is most likely to be separated from the lens by  $\sim 3$  AU for all the curves in Fig. 8. The steepest part of the curves indicating the highest probability density should then occur near where  $x_p = 3\text{AU}/\langle R_E \rangle$ . From Fig. 7,  $\langle R_E \rangle \approx 0.8, 2.05$  AU at  $\zeta = 0.2, 1.2$  respectively,

and we see that the steepest slopes indeed occur near  $x_p = 3 \approx 3\text{AU}/0.8\text{AU}$  for  $\zeta = 0.2$  and near  $x_p = 1.5 \approx 3\text{AU}/2.05\text{AU}$  for  $\zeta = 1.2$ . Another way to look at the behavior of  $F(x_p, a, \zeta)$  in Fig. 8 is to notice that for small  $\zeta$ ,  $\langle R_E \rangle$  is small so there is a greater probability of finding the planet at larger values of  $x_p$ . The consistencies in the positions of the curves as a function of the parameters in both Figs. 6 and 8 give one some confidence that the cumulative probabilities are correctly averaged.

The following describes how the integral of the probability density over the area swept in the lens plane out by the contours of  $2/(S/N)$  fractional perturbation of the light curves is carried out using  $F(x_p, a, \zeta)$ . This is the integral of  $dF(x_p, a, \zeta)/dx_p$  in Eq. (3). Assume for the present that the normalized distances from the lens to the inner and outer traces of the amplification contour extremes in upper half plane of Fig. 2 are  $r_1/R_E$  and  $r_2/R_E$  respectively. Since  $F(x_p, a, \zeta)$  is the averaged cumulative probability of finding the projected position of the planet in the annular region between  $x_p$  and  $a/R_E$  centered on the lens, the probability of finding the planet in a narrow wedge of angular width  $\Delta\theta$  and lying between  $r_1/R_E$  and  $r_2/R_E$  is just  $[F(x_p = r_1/R_E, a, \zeta) - F(x_p = r_2/R_E, a, \zeta)]\Delta\theta/2\pi$ . The probability of finding the planet in the area inside the two trace curves is then the sum of these probabilities for all the positions of the source as it is stepped through the encounter. A similar procedure determines the probability that the projected position of the planet lies in the area enclosed by the trace curves in the lower half plane of Fig 2. The sum of these two probabilities is the probability of detecting the planet during this particular encounter. This probability is of course dependent on the estimate of the  $S/N$  (Section 2) we use to define the perturbation contours of detectability in, for example, Figs. 2, 3 and 5.

## 5. Procedure

For each impact parameter, the source is located by its angular position  $\theta$  measured from the point of closest approach to the lens, and the source is stepped along its trajectory in equal increments  $\Delta\theta$ . The first point is the first encounter of the source with the Einstein ring of the lens where the unperturbed amplification  $A_0 = 1.34$ , which is here assumed to be the minimum amplification for an alert to the event. The brightness of the source is increased by the instan-

taneous amplification to determine the  $S/N$  at that position. The extremes in the contours corresponding to the perturbation of  $2/(S/N)$  are calculated for that  $S/N$  as outlined above and in Appendix B, and the probability that the planet lies in the wedges of angular width  $\Delta\theta$  along the source-lens line and between the extreme curves allowing detection is calculated for a particular semimajor axis. These “wedge” probabilities are summed for the encounter out to a source position along its trajectory of  $2R_E$  beyond its point of closest approach. The detection probability is determined for each of a distribution of approximately thirty impact parameters for the given source distance and magnitude, and averaged over the impact parameters.

The calculation is repeated for each of 11 semimajor axes ( $0.6 < a < 10$  AU), and one obtains a series of functions of  $a$ , labeled by the  $I$  magnitude of the source at the distance  $\zeta$ . These are probabilities  $P(a, \zeta, I)$  of detecting the planet during the event averaged over the MF of the lenses, over the distribution of the lenses along the particular LOS from the observer to the source at  $\zeta$ , and over the distribution of impact parameters. Figs. 9 and 10 show examples of these curves for  $\zeta = 0.2$  and 1 respectively for a selection of source  $I$  magnitudes. In these figures,  $q = 0.001$ , the LOS is toward Baade’s window  $(\ell, b) = (1^\circ, -4^\circ)$  and the extinction  $A_{I8} = 0.76$  mag (Holtzman *et al.* 1998). At  $\zeta = 0.2$ , the brightest star in the LF has  $I=7.16$ , and the curves for  $7.16 < I \lesssim 14.5$  are superposed, because for these bright stars,  $S/N$  exceeds 200 for a 60 sec integration time, and we have assumed the integration is reduced so that  $S/N$  does not exceed 200 in such circumstances. This means that the detection probability is observationally controlled to be the same for the given LOS and parameter values for all sources with  $I \lesssim 14.5$ . Otherwise, the detection probability increases with source brightness in these figures because the higher  $S/N$  increases the area contained within the curves tracing the extremes in the amplification contours as shown in Fig. 3.

We pointed out above that the probability distribution of the projected position of the planet on the lens plane is strongly peaked near  $r = a$ , and because the perturbation of the light curve decreases monotonically as the planet is moved radially away from the Einstein ring radius in either direction (provided it is outside the closed critical curves), the probability of detection is maximized when the planet is near

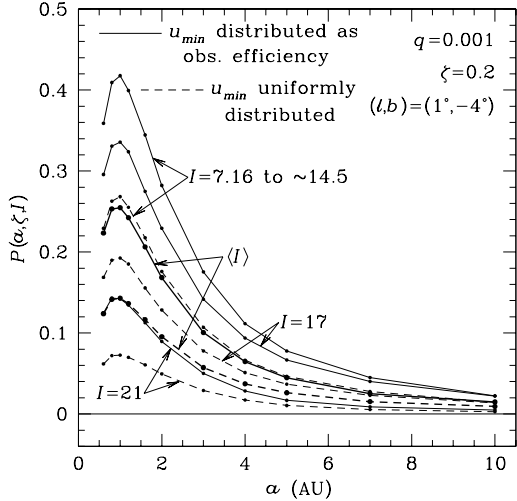


Fig. 9.— Probability  $P(a, \zeta, I)$  (thin lines) of detecting a planet when the source at  $\zeta = 0.2$  for a selection of source magnitudes plus the average of the probabilities over the LF  $P(a, \zeta)$  (heavy lines).  $I = 7.16$  is the brightest star in the LF for  $A_{I_8} = 0.76$ , and a single curve applies for  $I = 7.16$  to about 14.5 because of our constraint that  $S/N$  not exceed 200. The probability has been averaged over the LOS distribution of lenses, over the Holtzman *et al.* mass function, and over the distribution of impact parameters  $u_{min}$ , where the Zhao bulge model and the Bahcall-Soneira disk model are assumed for the stellar mass distribution in the Galaxy.

the Einstein ring of the lens. One then expects the probability of detection to be maximized when the semimajor axis of the planet is near the average value of the Einstein ring radius between the observer and the source location. From Fig. 7, at  $\zeta = 0.2, 1.0$ ,  $\langle R_E \rangle \approx 0.85, 1.7$  AU for the Holtzman *et al.* (1998) MF, where relatively small values result from the dominance of M stars in the MF. Correspondingly, the peak in the detection probabilities occur near (1 AU, 2 AU) for  $\zeta = (0.2, 1.0)$

The probabilities are shown for two distributions of impact parameters in Figs. 9 and 10. The random nature of the events means that the impact parameters will be uniformly distributed, where we choose  $0 < u_{min} < 1$  with  $u = 1$  corresponding to an amplification of 1.34 being the assumed threshold for an

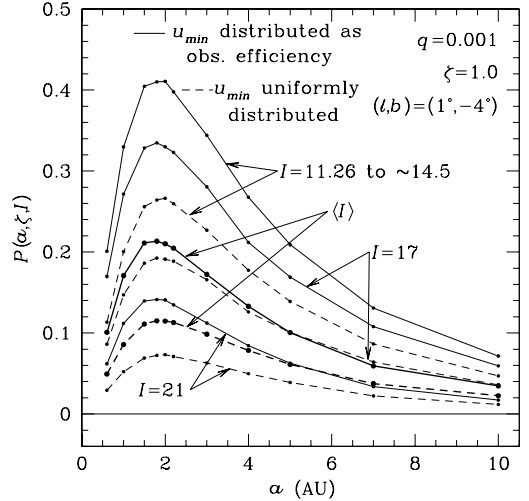


Fig. 10.— Same as Fig. 9 except the source is at  $\zeta = 1.0$  and the brightest star in the LF is  $I = 11.26$ .

alert. However, events with smaller impact parameters are more likely to be observed because of the higher magnifications, so the distribution of impact parameters of recorded events will be biased toward the smaller values. Accordingly, the second distribution of  $u_{min}$  is that of Fig. 9 from Alcock *et al.* (2000), which has a higher proportion of small impact parameters to reflect the observational efficiencies. In fact, events with  $u_{min} > 0.9$  contribute negligibly to the average of the probabilities over the distribution of  $u_{min}$ , so we choose 30 values  $0.01 \leq u_{min} \leq 0.91$  for the uniform distribution. The distribution determined by observational efficiencies naturally reduces the number of larger impact parameters in the range  $0 < u_{min} < 1$ . The higher probabilities for this latter distribution of  $u_{min}$  reflect the higher probabilities for closer impact parameters implied in Figs. 2 and 5.

Also shown in Figs. 9 and 10 are the averages over the distribution of  $I$  magnitudes of the sources at each distance. These are effectively averages over the LF expressed in  $I$  magnitudes appropriate to each distance but truncated to the visible sources ( $I < 21$ ). The averaged probability is

$$P(a, \zeta) = \int_{I_{min}}^{21} P(a, \zeta, I) f_L(I) dI, \quad (8)$$



where  $I_{min} = 10.5 + A_{I8}\zeta + 5 \log \zeta$  and  $f_L(I)$  is  $f_L(I_8)$  in Eq. (A5) with Eq. (5) replacing  $I_8$  and the result renormalized so that  $f_L(I)dI$  represents the fraction of *visible* sources in range  $dI$  about  $I$ . Examples of  $P(a, \zeta, I)$  are the labeled curves in Figs. 9 and 10, and  $P(a, \zeta)$  is labeled with  $\langle I \rangle$ . Since the curves are for discrete values of  $I$ , the integral in Eq. (8) is approximated by  $\sum_i P(a, \zeta, I_i) f_L(I_i) \Delta I_i$ , where  $I_i$  are the discrete values of  $I$  at which  $P$  is evaluated and  $\Delta I_i$  is an increment centered on  $I_i$  and stretching halfway to adjacent values of  $I_i$  on either side. Fig. 11 demonstrates this procedure, where the shaded area under the histogram is the average over the LF for  $\zeta = 1$  and  $a = 2.2$  AU. Fig. 12 shows the detection probability averaged over the luminosity function of the sources for the uniform distribution of impact parameters, over the Holtzman *et al.* MF and over the LOS distribution of lenses for a series of values of  $\zeta$ . The semimajor axis where the probability is maximal follows the mean value of  $R_E$  as described above. The derivation of the overall averaged detection probability will be completed by the average over the distribution of visible sources.

## 6. Average of $P(a, \zeta)$ over $\zeta$

The final average of the detection probability is carried out with the following expression:

$$P(a) = \frac{\int_{0.1}^{1.2} P(a, \zeta) n_s(\zeta) \zeta^2 \xi(\mathcal{F}_{21}, \zeta, A_{I8}) d\zeta}{\int_{0.1}^{1.2} n_s(\zeta) \zeta^2 \xi(\mathcal{F}_{21}, \zeta, A_{I8}) d\zeta}, \quad (9)$$

where  $n_s(\zeta)$  is the number density of sources at distance  $\zeta$  and where

$$\xi(\mathcal{F}_0, \zeta, A_{I8}) = C_1 (4\pi D_8^2 \mathcal{F}_{21} \zeta^2 e^{-0.921 A_{I8}})^\beta + C_2, \quad (C11)$$

derived in Appendix A, is the fraction of the sources with observed flux densities  $\mathcal{F}$  greater than a minimum  $\mathcal{F}_{21}$  assumed detectable.  $\mathcal{F}_{21} = 6.21 \times 10^{-15}$  ergs  $\text{cm}^{-2} \text{sec}^{-1}$  is the minimum flux density in  $I$ -band considered observable—here from a star with  $I = 21$ .  $C_1 L_{I0}^\beta + C_2$  is the fraction of the sources with luminosity  $L_I > L_{I0}$ , which follows from the fraction of sources with  $I < I_0$  found from the LF in Appendix A. The constants and index are different in the LF for each of three ranges of  $I_8$  (Eq. (A5)) with 1.16% of the stars having  $I_8 < 17$  and 4.18% of the stars having  $I_8 < 18.5$ , with  $I = 17$  and 18.5 being the values where the LF index changes. Hence,  $C_1$ ,  $C_2$  and  $\beta$

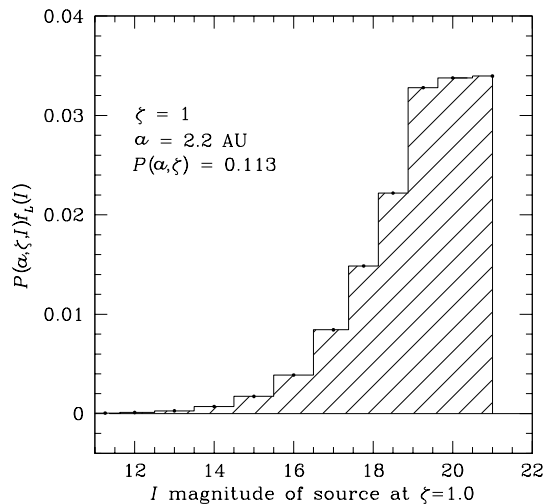


Fig. 11.— An example of the average of the detection probabilities over the LF for  $\zeta = 1$  and  $a = 2.2$  AU. The probabilities have already been averaged over the distribution of lenses along the LOS, over the Holtzman *et al.* mass function and over a uniform distribution of impact parameters. The shaded area under the histogram is the averaged probability, which is 0.113 in this case.

must change when  $\xi = 0.0116$  and 0.0418. Also  $\xi = 1$  for values of  $\zeta$  so small that all of the sources are visible and  $\xi = 0$  for values of  $\zeta$  so large that even the brightest source in the LF has  $I > 21$ . The parameters in  $\xi$  and examples of values of  $\zeta$  where changes occur for a few values of  $A_{I8}$  are given in Appendix A. Fig. 13 shows  $\xi$  as a function of  $\zeta$  for three values of  $A_{I8}$ .

We choose source distances for which the detection probability is to be determined to range from  $\zeta = 0.1$  to 1.2 in increments of 0.1. It is very unlikely for any source to be closer to us than  $\zeta = 0.1$  (0.8 kpc), and beyond  $\zeta = 1.2$ , extinction and blending will probably make the number of sources that are useably visible negligibly small. The source number density along the LOS is obtained from the Zhao (1996) bulge model and the Bahcall-Soneira disk for the Holtzman *et al.* (1998) mass function in Appendix B. The overall coefficients in the bulge and disk distributions are determined by the constraints on the total bulge mass of  $2.2 \times 10^{10} M_\odot$  (Zhao, 1996) and a local disk mass

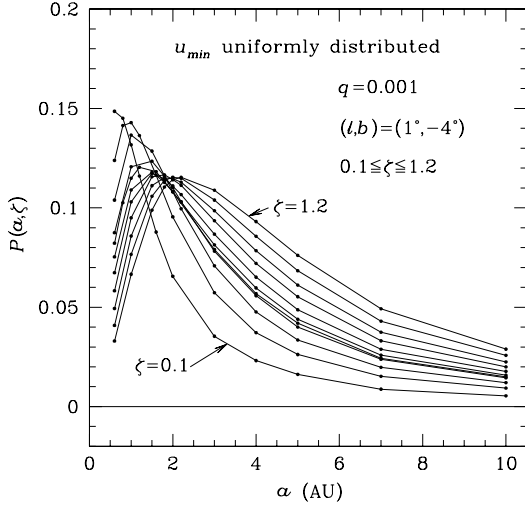


Fig. 12.— Average of the detection probability over the LOS distribution of lenses, over the Holtzman *et al.* MF, over a uniform distribution of impact parameters  $u_{min}$ , and over the LF for  $\zeta$  incremented in steps of 0.1 (except  $\zeta = 0.4$  is not included). The peaks occur where  $a \approx \langle R_E \rangle$ .

density of  $0.05M_{\odot}\text{pc}^{-3}$  (Bahcall and Soneira, 1980) respectively. The functions  $P(a, \zeta)$  (E.g., Fig. 12) are made continuous functions of  $\zeta$  by interpolating between the discrete points where they are evaluated. This makes the integrands for a given LOS in Eq. (9) functions of  $\zeta$  alone and evaluation of the integrals is straightforward.

Fig. 14 shows the averaged probability  $P(a)$  for a uniform distribution of impact parameters and for that distribution appropriate to the efficiency of detection by the MACHO group (Alcock *et al.*, 2000). The line of sight is toward Baade’s window  $(\ell, b) = (1^{\circ}, -4^{\circ})$ , where  $A_{I8} = 0.76$  (Holtzman *et al.* 1998). The higher weight given to the small impact parameters in the latter distribution nearly doubles the probability of detection obtained from a uniform distribution of  $u_{min}$ . The large probabilities at small planet separations that resulted for small  $\zeta$  (Fig. 12) are seen to be suppressed by the lack of sources at small  $\zeta$ . The semimajor axis for the peak probability of detection is near 1.5 AU, which is close to the mean  $R_E$  over the entire LOS for the Holtzman, *et al.* mass function and Zhao plus Bahcall-Soneira galactic model.

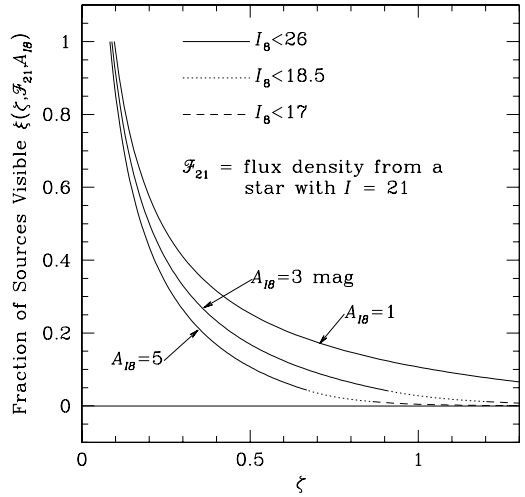


Fig. 13.— Fraction of sources visible for the adopted LF as a function of source distance.  $\mathcal{F}_{21}$  is the flux density from a star with  $I$ -magnitude = 21 that is assumed to be the minimum observable, and  $A_{I8}$  is the  $I$ -band extinction to 8 kpc. The different line types correspond to the different forms of the LF for different brightness ranges.

## 7. Parameter dependence of the detection probability

Fig. 15 shows the reduction in the probability by increasing the extinction to  $A_{I8} = 3$ , by assuming a  $3\sigma$  instead of a  $2\sigma$  detection both along the LOS to Baade’s window and by changing the LOS to  $(\ell, b) = (10^{\circ}, -4^{\circ})$  with  $A_{I8}$  restored to 0.76 mag. All assume the distribution of  $u_{min}$  appropriate to the efficiency of observing the event, and this curve for Baade’s window and  $A_{I8} = 0.76$  is repeated from Fig. 14 for comparison. The  $3/(S/N)$  detection criterion reduces the probability of detection for all semimajor axes over that for a  $2/(S/N)$  detection criterion as expected, and the mechanism is a reduction in the area in the lens plane inside of which a planet’s projected position would lead to a detection. Changing the line of sight to  $(\ell, b) = (10^{\circ}, -4^{\circ})$  (also with the  $3/(S/N)$  detection criterion) from  $(\ell, b) = (1^{\circ}, -4^{\circ})$  with equal extinctions increases the probability of detection for  $a \gtrsim$  its value corresponding to the peak probability and decreases the probability for  $a \lesssim$  its value near the peak. By swinging the LOS away from the

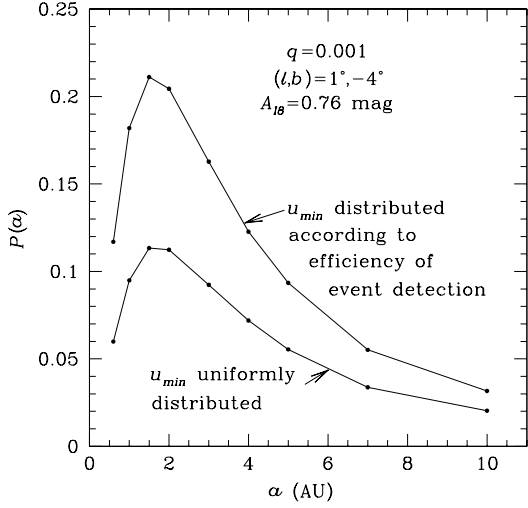


Fig. 14.— Averaged probability of detecting a planet during a microlensing event toward Baade’s window for a uniform distribution of impact parameters and a distribution determined by the observational efficiency of the MACHO group (Alcock *et al.* 2000).

bulge, we have effectively increased the mean Einstein ring radii of the lenses. There are considerably fewer sources and fewer lenses at the most distant parts of the LOS at the larger Galactic longitudes, so there is less weight given to those configurations of small Einstein ring radii in the averages over both the lens and source distributions. That means that planets with small semimajor axes (near  $R_E$  where the probability is large) will have a smaller probability of detection, whereas those with larger semimajor axes will have their averaged probabilities increased. One can see from Fig. 15 that this is not a large effect. The increase in  $A_{I8}$  toward Baade’s window has the effect of increasing the apparent magnitudes of all the sources, thereby reducing the  $S/N$  and the probability of detecting a planet.

Fig. 16 emphasizes the effect of changing the line of sight relative to the center of the Galaxy. Here a series of LOS with different Galactic latitudes and the same Galactic longitude ( $\ell = 1^\circ$ ) again show the effect of decreasing or increasing the proportion of the lenses for large distances from the observer. The probability of detection is raised for larger semima-

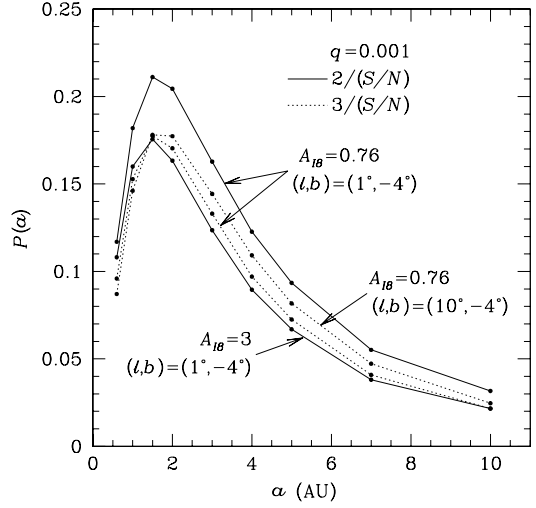


Fig. 15.— Averaged probability of detecting a planet during a microlensing event showing effect of shifting the LOS, of increasing the extinction, and of using a  $3/(S/N)$  instead of a  $2/(S/N)$  detection criterion. The probability is averaged over the source-lens impact parameter distribution determined by the observational efficiency, over the lens distribution along the LOS, over the MF, over the LF, and over the visible source distribution along the LOS.

for axes for the LOS directed further from the high spatial density region near the Galactic center, and it is lowered for the LOS closer to the Galactic center for reasons discussed above. Rather than show the complete averaged probability for these examples, we notice that the probability averaged only over the distribution of impact parameters, over the distribution of lenses along the line of sight to  $\zeta = 1.0$  and over the MF for  $I = 19.5$  mag gives a good approximation to the detection probability with additional averages over the LF and the distributions of sources leading to  $P(a)$ . The points indicated by stars in Fig. 16 are appropriate to  $P(a)$  and indicate how well the partial average for the selected values of  $\zeta$  and  $I$  approximates the total average for  $(\ell, b) = (1^\circ, -4^\circ)$ .

The peak probability, in addition to being shifted slightly to larger semimajor axes as  $|b|$  is increased, is also increased slightly. This is an extension of the increase in probability for larger semimajor axes as less weight is given to the more distant lenses with in-

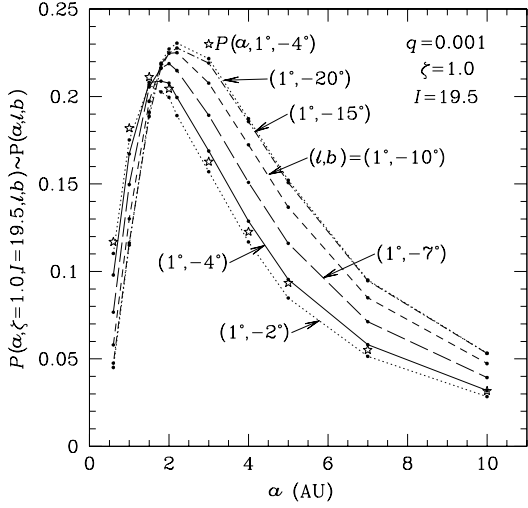


Fig. 16.— Averaged probability of detecting a planet during a microlensing event showing the effect of shifting the line of sight along a line of constant galactic longitude  $\ell = 1^\circ$ . Here  $P(a, \zeta, I)$ , with  $\zeta = 1$  and  $I = 19.5$ , is used to approximate  $P(a)$ , where the galactic coordinates have been added in the arguments to distinguish the LOSs. The stars correspond to  $P(a) \equiv P(a, 1^\circ, -4^\circ)$  and indicate the good approximation by the partial average for the selected  $I$  magnitude for  $(\ell, b) = (1^\circ, -4^\circ)$ .

creasing  $|b|$ . Since the averaged probability depends in an intricate way on the weighting of the Einstein ring radius by the distribution of lenses along the LOS relative to the semimajor axis of the planetary orbit, there is no reason to expect the peak probability not to change as it shifts to larger semimajor axes. There is almost no difference in the probability in Fig. 16 for  $b = -15^\circ$  and  $-20^\circ$ . The LOS for these latitudes does not intercept much of the bulge distribution of stars, so the distribution of lenses along the LOS, being mostly disk stars, changes very little between  $b = 15^\circ$  and  $20^\circ$ .

The reason for considering the modified Holtzman *et al.* mass function in Fig. 7 is that more M stars than are observed seem to be required in the MF to account for the relatively large number of short time scale events toward the Galactic center. The modified Holtzman mass function  $\propto M^{-2.2}$  for all stars  $0.08 \leq M \leq 2.0M_\odot$  gives a reasonably good ap-

proximation to the time scale frequency distribution obtained by the MACHO group for the 1993 bulge season (Peale, 1998), but extending the MF into the brown dwarf region does not (Peale, 1999). The larger number of small mass stars in this distribution leads to the reduction in the averaged Einstein ring radius for all  $\zeta$  in Fig. 7. Its consideration here allows us the opportunity to illustrate the effect of changing the mass function on the probability of planet detection. We expect this reduction in the mean Einstein ring radius to shift the peak in the probability distribution to smaller semimajor axes, to lower the probability for the larger semimajor axes, and to raise it for the smallest semimajor axes as discussed above. This expected effect is shown in Fig. 17, where we have again used the partial average of the detection probability as an approximation to  $P(a)$ . The peak probability has moved from something near 1.8 AU to being near 1.4 AU, again showing that the peak occurs near the averaged Einstein ring radius  $\langle R_E \rangle \approx 1.4$  for the largest values of  $\zeta$  in Fig. 7 (lower curve).

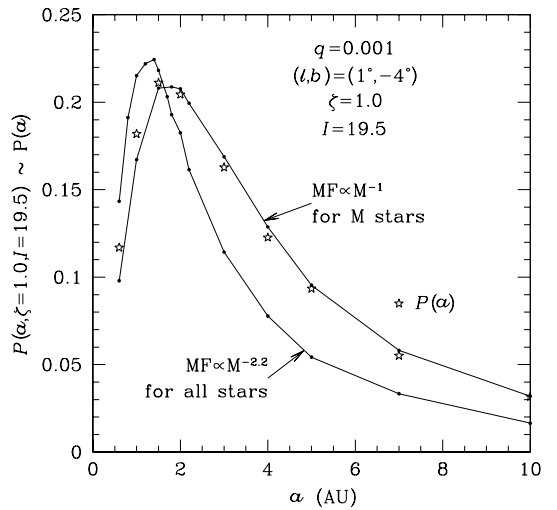


Fig. 17.— Effect on the averaged detection probability of changing the MF. The other information is the same as in Fig. 16. The larger number of M stars in the MF with the larger index leads to a shift in the peak probability to smaller  $a$  because of the smaller  $\langle R_E \rangle$ . This same shift in  $\langle R_E \rangle$  to smaller values leads to a decreased probability for large  $a$  and an increased probability for small  $a$ .

The averaged probability of planet detection varies approximately as  $\sqrt{q}$ . This is shown in Fig. 18, where decreasing  $q$  by a factor of 10 leads to a reduction in the probability of about  $\sqrt{10}$ . The actual ratio of the probabilities for the two values of  $q$  starts at 3.14 for  $a = 0.6$ , drops to 2.7 near the peak and rises to 5.7 for  $a = 10$ , which shows that the approximate scaling is rather crude for some values of  $a$ , but it still gives a useful extension of the results for  $q = 0.001$  and 0.0001 shown in Fig. 18. This scaling should not be carried to mass ratios less than  $10^{-4}$ , since effects of the non-zero size of the source become important and are not included in this analysis (*e.g.*, Bennett and Rhie, 1996). On the other hand, the probabilities so obtained may not be that far from the Bennett and Rhie values for small planets (Peale, 1997). The source of this scaling can be traced to the scaling of the size of the contours of equal perturbation in Figs. 2 and 5 approximately as  $\sqrt{q}$  (Gould and Loeb, 1992). The length of the arc described by the center of the contours during the event is independent of  $q$ . So only the dimension of the total area swept out by the contours that is perpendicular to this arc is affected by  $q$ . As this dimension scales approximately as  $\sqrt{q}$ , the whole area swept out scales approximately as  $\sqrt{q}$ . Since the probability per unit area of the projected position of the planet falling into the area usually does not vary much over the area, the total probability of finding the planet in the area scales roughly as the area and hence  $\sim \sqrt{q}$ .

We have averaged over the LF in the above probabilities, but since the magnitude of the source is known in any particular event, we could eliminate this average and evaluate the detection probability for particular  $I$  magnitudes. These probabilities are shown in Fig. 19. The probabilities for fixed  $I$  magnitudes averaged over the distribution of lenses along the LOS, over the lens MF, over the distribution of impact parameters (here determined by observational efficiency), and over the distribution of visible sources along the LOS are higher for brighter stars because of the increasing  $S/N$  with decreasing  $I$ -band magnitude. As in the other examples, the probabilities are significant even for the faintest stars that we have assumed suitable for followup photometry from the ground.

The peak amplification during an event will yield the impact parameter with an accuracy determined by how well the blending can be modeled, so the average over  $u_{min}$  can also be eliminated for individual

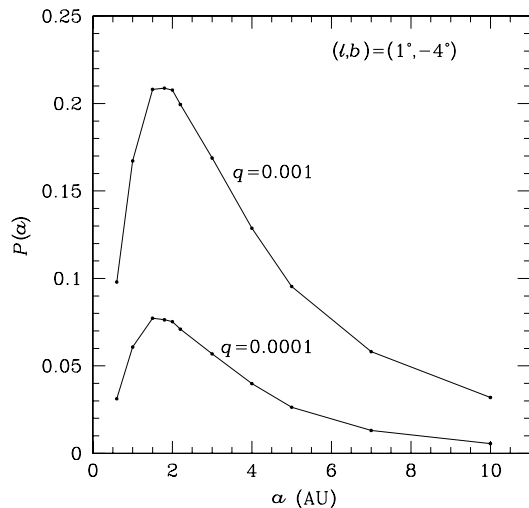


Fig. 18.— Effect on the completely averaged detection probability of changing the planet-star mass ratio  $q$  showing that  $P(a) \sim \sqrt{q}$ . The actual ratio between the two curves is 3.14 at  $a = 0.6$ , decreases to 2.7 near the peak and increases to 5.7 at  $a = 10.0$ , so the scaling is poorest at the larger values of  $a$ .

events. Fig. 20 shows the detection probabilities for individual events involving a 19th magnitude source with impact parameters  $u_{min} = 0.1$  and 0.3. The probabilities are now averaged only over the degenerate parameters of the distances to the lens and source, weighted by the distribution of lenses and sources along the LOS, and the MF. The rapid drop in the detection probability as the impact parameter is increased is evident, and it again illustrates how the bias toward small impact parameters in the observational record increases the completely averaged probability of detection in Fig. 14.

Since Fig. 20 is based on idealized observational conditions, it is probably of limited use in interpreting real microlensing data from an individual event. However, the techniques developed here can be used in the interpretation of the Gaudi and Sackett (2000) analysis of null results from real data (Albrow *et al.* 2000b) by eliminating the guesses at representative source and lens distances. The  $\chi^2$  analysis of Gaudi and Sackett outlined in Section 1 yields a best estimate of the impact parameter and source  $I$  magnitude, which we shall assume as known for the prob-

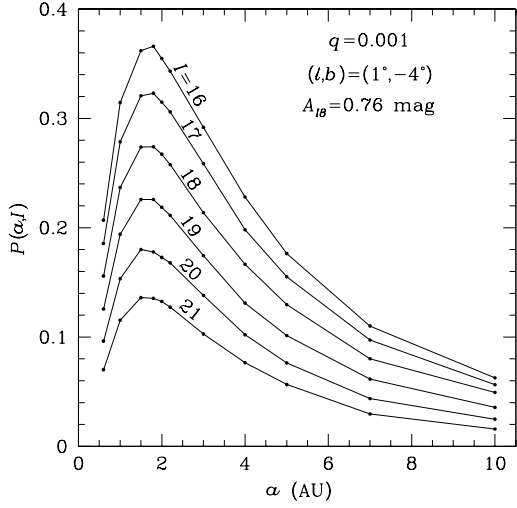


Fig. 19.— Averaged detection probability as a function of the  $I$  magnitude of the source for the LOS toward Baade’s window. The average over the LF is bypassed here and  $P(a) \rightarrow P(a, I)$  on the vertical axis. The impact parameter  $u_{min}$  is distributed according to the efficiency of event detection. The Holtzman et al. (1998) mass function is assumed.

ability  $\epsilon(x_p, q)$  in Eq. (2). Like Fig 20, this eliminates averages over  $u_{min}$  and over the LF of the sources in Eq. (3). The elimination of the LF average means the integration over the distribution of sources can be included with the integration over the distribution of lenses and over the MF. The point where  $q$  enters the averaging process is in the integration of  $dF(x_p, a, \zeta)/dx_p$  in Eq. (3) over the area  $S(I, u_{min}^i)$  inside of which a planet would be detected, since  $q, I, u_{min}$  determine the extent of the area. To determine the probability of detecting a planet with a particular mass ratio  $q$  at semimajor axis  $a$  for the real data from a particular event,  $\epsilon(x_p, q)$  is integrated over the probability density  $-dF(x_p, a)/dx_p$  over the range of  $x_p$  where the density is non-negligible and for which  $\epsilon(x_p, q)$  has been determined from the data. Note that  $\zeta$  is missing from the arguments of  $F(x_p, a)$  since we have also integrated over the distribution of source distances weighted by the source distribution. Hence,

$$P'(a, q) = \int_{x_{pmin}}^{x_{pmax}} dx_p \epsilon(x_p, q) \left( -\frac{d}{dx_p} \right)$$

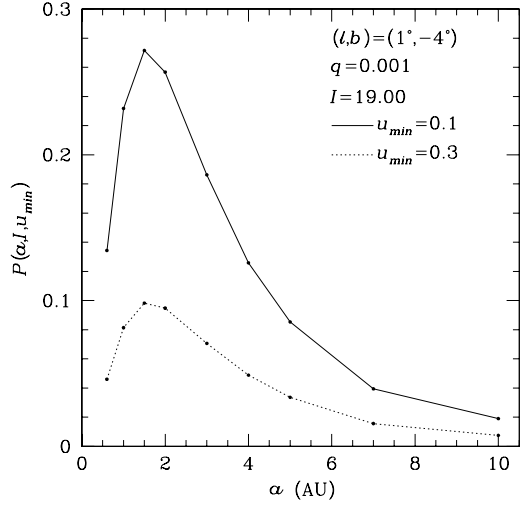


Fig. 20.— Probability of detecting a planet during an individual event where both the impact parameter and the  $I$  magnitude of the source are known. The averages over the impact parameter distribution and over the LF are omitted, leaving only averages over the degenerate parameters,  $z, \zeta$  and  $M$ , where the former two are weighted by the distribution of lenses and sources along the LOS and the last by the MF.  $P(a) \rightarrow P(a, I, u_{min})$  on the vertical axis. Note the rapid drop in the detection probability as the impact parameter is increased.

$$\begin{aligned} & \times \int_{0.1}^{1.2} \int_0^\zeta \int_{M_{min}}^{M_{max}} n'_s(\zeta) n'_L(z, M) \\ & \times \Theta[f(x_p, a, \zeta, z, M)] F(x_p, a, \zeta, z, M) d\zeta, dz dM, \end{aligned} \quad (10)$$

is the probability of detecting a planet with mass ratio  $q$  at semimajor axis  $a$  for the particular event whose data were used in the  $\chi^2$  analysis to yield  $\epsilon(x_p, q)$ . The variables in Eq. (10) are defined just below Eq. (3). The integral is repeated for a sufficient number of values of  $a$  to define the functional form of  $P'(a, q)$ . The integrals are to be evaluated with a Monte Carlo technique as before. It should be noted that  $\epsilon(x_p, q)$  depends only on the data and is model independent, whereas  $P'(a, q)$  depends on MF, and the lens and source distances weighted by the lens and source distributions along the LOS, and finally  $P(a, q = 0.001)$  in Eq. (9) depends on all of these parameters plus the LF of the sources and the distribution of impact

parameters.

## 8. Summary

We have derived the probability of detecting a planetary companion of a star acting as a gravitational lens of a more distant star toward the Galactic bulge sometime during the microlensing event. The probability is determined as a function of the orbital semimajor axis of the planet, and it is based on a criterion which assumes that a perturbation to the microlensing light curve due to the presence of the planetary companion that exceeds  $2/(S/N)$  for at least 20 consecutive photometric data points is detectable. By the observer’s choice under the assumption that many events are being monitored simultaneously and the likely dominance of systematic noise for brighter stars, integration times are assumed to be terminated when  $S/N$  exceeds 200. Given this criterion, the probability for  $q = 0.001$  (or 0.0001) is averaged over the distribution of the projected position of the planet relative to the lens, over the spatial distribution of the lenses along the LOS for a model of the Galaxy incorporating the Zhao (1996) and the Bahcall-Soneira (1980) bulge and disk model respectively, over the Holtzman *et al.* (1998) mass function, over the distribution of source-lens impact parameters inside the Einstein ring radius  $R_E$ , over the  $I$ -band LF derived from the  $J$ -band LF of Zocalli *et al.* (2000) as adjusted by the source distance and the extinction thereto, and over the spatial distribution of sources along the LOS, which is identical to the distribution of lenses except only a fraction are visible due to distance and extinction.

The averaged probability scales approximately as  $\sqrt{q}$  (Fig. 18), but the scaling should not be extended to values of  $q \lesssim 10^{-4}$  where the effect of the non-zero size of the sources becomes important. The detection probability has its maximum value of a little over 10% if a uniform distribution of impact parameters is assumed and over 20% if the distribution of impact parameters is adjusted for the observing efficiency found by Alcock *et al.* (2000) (Fig. 14). The maximum occurs for a planet semimajor axis that is close to the average value of  $R_E$  over the LOS—1.5 to 2 AU for a LOS toward Baade’s window  $(\ell, b) = (1^\circ, -4^\circ)$  for the Holtzman *et al.* (1998) MF. The averaged probability of detection is decreased with increasing extinction, because of the lowered  $S/N$  for all sources. Requiring a detectable perturbation of the light curve to

be  $3/(S/N)$  rather than  $2/(S/N)$  decreases the probability by about 20% (Fig. 15). If the probability is not averaged over the LF, the otherwise averaged probability increases with source brightness because of the higher  $S/N$  (Fig. 19). A MF with a higher proportion of M stars shifts the peak in the probability to smaller semimajor axes as expected (Fig. 17). It also reduces the probability of detecting a planet at large semimajor axes while increasing the probability of detecting planets at very small semimajor axes. These trends are a consequence of the reduced  $\langle R_E \rangle$ , where preference for semimajor axes comparable to  $R_E$  result from highest probability of detecting a planet occurring when its projected position is near  $R_E$ . These same trends in the probability are seen when the LOS is moved away or toward regions of high source density near the Galactic bulge (Figs. 16 and 15), where the cause is again the change in  $\langle R_E \rangle$  because of the different weightings of the source and lens distributions in the averages for different LOSs.

For individual events, good estimates of the impact parameter and the magnitude of the source are usually available. The averages over the impact parameter distribution and over the LF are then omitted in determining the probability of detection for a particular event leaving averages only over the degenerate parameters. The drop in detection probability with impact parameter for a 19th magnitude source is illustrated in (Fig. 20). For real individual events, the empirically determined, model independent probability  $\epsilon(x_p, q)$  is averaged over probability density  $-dF(x_p, a)/dx_p$  to yield  $P'(a, q)$ , the probability of detecting a planet with given planet-star mass ratio  $q$  at semimajor axis  $a$  for that particular event.

## 9. Discussion

All of the variations of parameters we have investigated maintain the relatively high detection probabilities over a substantial range of semimajor axes, while shifting the peak slightly and altering the relative probabilities of detecting planets with large and small semimajor axes. This relative robustness reinforces the optimism for planet detection through microlensing generated by the Gould and Loeb (1992) paper. Continuous coverage of the light curve is assumed, whereas weather and hardware maintenance limit the Galactic bulge coverage by even a global distribution of 3 or 4 telescopes to a maximum near 80% at the midpoint of the bulge season, and this

falls off on either side of mid season because a smaller fraction of the night is usable (Peale, 1997). Still, for Jupiter and Saturn mass planets, defined in terms of the planet-star mass ratio, the perturbation will last on the order of one day and would usually be detected, although the light curve during the perturbation would not be completely covered. If breaks in the coverage exceed one or two days at a time, the probability of planet detection will be reduced by the percentage of total event time that is missed. Our detection criterion for a perturbation of magnitude  $2/(S/N)$  persisting for at least 20 consecutive data points means that missed coverage during the perturbation is serious for detection and much more so for determining  $q$ .

Necessarily, we have simplified the calculation of  $S/N$  for unknown observing systems. The  $S/N$  from photon statistics and sky background is reduced by a factor 1/4 to account for systematic and other neglected noise sources. The factor was chosen to yield the empirical  $S/N$  values for two real systems with their observing conditions. Although this yields reasonable  $S/N$  estimates for our purposes, each system must be separately calibrated, and this constrains other parameters such as integration time for desired  $S/N \approx 100$  or more. Increased integration time may compromise the desired sampling time of a data point every one or two hours if there are too many ongoing events that must be monitored. Either the overall probability of planet detection would be thereby reduced, or the number of events that can be adequately followed with high  $S/N$  will be limited in a ground based search. The averaged detection probabilities thus explicitly depend on our assumptions of a 2 m telescope, 1.4 arcsec seeing, and a fixed integration time of 60 seconds, because of their determination of  $S/N$  for a given magnitude source.

We have neglected blended light under the assumption that image subtraction techniques (Alcock *et al.* 2000) can eliminate this contamination for a wide range of source magnitudes and lensing magnifications. If unmodeled blended light remains, it will have the effect of decreasing the fractional perturbation of the light curve by the planet and reducing the probability of detection in addition to introducing an uncertainty in the impact parameter. Several parameters, such as integration time, are not going to be fixed as we have assumed, but will vary even during a single night as conditions change. We have also assumed the single lens light curve is known a priori,

when only a light curve that is the best fit to the data will be available.

The complete averages of the planet detection probabilities we have derived, in addition to establishing the robustness of their relatively large values, are useful in determining the effect of various distributions of parameter values. For establishing the meaning of null results, however, all the information available for each particular event should be used. Averaged values should be used only for those properties of the lens-source system that cannot be lifted from the degeneracies. The magnitude of the source is going to be more or less known, so averages over the LF are not appropriate in analyzing individual events. The peak amplification will yield the impact parameter with an accuracy determined by how well the blending can be modeled, so the average over  $u_{min}$  should also be eliminated for individual events. We have shown how the probability varies for various magnitude sources, but averaged over all other parameters in Fig. 19, and Fig. 20 shows how the probability decreases for individual events as the impact parameter is increased. This decrease can be also be estimated from Fig. 4. The degeneracies remaining are the distances to the lens and source and the mass of the lens, so for most events, averages over the distribution of lenses and sources along the LOS and over the MF are still appropriate. One or more of these averages might be removed for individual events if the parallax of the lens can be determined.

There have been several comparisons of the microlensing technique for the detection of planets with the very successful radial velocity technique (*e.g.*, Albrow *et al.* 2000b), where the emphasis has been on their complementary detection of distant and close planets respectively or microlensing's unique sensitivity to terrestrial mass planets. Microlensing's advantage for detecting large, distant planets from the ground and compiling meaningful statistics therefrom decreases as the time span for the radial velocity programs with the highest precision increases. However, most of the lenses will be M stars, whereas these stars comprise only a small fraction of the radial velocity targets. In addition, the M stars will be located primarily in the Galactic bulge in contrast to the local nature of the stars in radial velocity searches. In that sense, microlensing searches from the ground will always have a unique contribution to make in constraining the statistical distribution of planets.

Its unique sensitivity to Earth mass planets may



be less important because of the reduced probability of detecting such planets from the ground. This importance would be drastically increased with the promise of an enormous increase in the number of events and the continuous monitoring of all the events with high time resolution, high precision photometry from space (Bennett and Rhie, 2000). Such a space based planet detection scheme using microlensing, if realized, would decrease the motivation for ground based searches because of the drastically increased throughput and higher sensitivity. However, no such mission has yet been funded, so it is premature to abandon continued planning for extensive ground based microlensing searches for planets. The robust nature of the large probabilities of detection for Jupiter to perhaps Uranus mass planets during an event demonstrated here supports the continuation of this effort. The need for the statistics of the occurrence of planets distant from their sources that can be obtained relatively rapidly from the ground only with a dedicated microlensing search will become more urgent as planning for various space-based planetary searches continues.

### Acknowledgements

It is a pleasure to thank Alex Filippenko, John Huchra, Penny Sackett and especially Tim Sasseen for information and instruction concerning photometric signal to noise ratios, Thanks also to Man Hoi Lee who read the entire manuscript and offered many suggestions for improvements. Thanks are due an unknown referee whose careful review and suggestions greatly improved the manuscript. Partial support for this work came from the NASA OSS and PG&G Programs under grants NAG5-7177 and NAG5-3646.

### A. The luminosity function

Zoccali *et al.* (2000) assemble a luminosity function (LF) for stars in the Galactic bulge in  $J$ -band from their own data for stars later than the main sequence turnoff and from Tiede *et al.* (1995) and Frogel & Whitford (1987) for the giants. We approximate the LF in their Fig. 10 with three straight line segments and further normalize the integral over the LF to unity such that

$$\begin{aligned} f_L(J) &= 2.628 \times 10^{-8} e^{0.748J}, & 9 \leq J \leq 17, \\ &= 1.108 \times 10^{-14} e^{1.612J}, & 17 \leq J \leq 18, \end{aligned}$$

$$= 6.096 \times 10^{-5} e^{0.366J}, \quad 18 \leq J \leq 24 \quad (\text{A1})$$

represents the fraction of sources per unit  $J$  magnitude. Although the extinction is lower in  $J$ , the sky noise may be too excessive in this band for either the initial microlensing survey or the high time resolution followup monitoring in search of planetary perturbations (C. Stubbs, private communication 1999). We will therefore convert the LF to  $I$ -band, for which we need  $I - J$  as a function of  $J$ . For this purpose, we use Tables II and III of Bessell and Brett (1988), which give the colors of dwarfs (Class V) and giants (Class III) respectively as a function of spectral type in terms of magnitude differences.

$V - J$  and  $I - J$  are determined as functions of  $M_V$  with appropriate relations among the columns in the tables, and  $M_V$  is substituted for the spectral types separately for dwarfs and giants.  $M_V$  values are taken from § 96 of Allen (1973). Linear fits to the points in the  $V - J$ ,  $M_V$  and  $I - J$ ,  $M_V$  planes yield

$$\begin{aligned} V - J &= 0.361 M_V - 0.422 & \text{for dwarfs,} \\ &= -1.833 M_V + 2.667 & \text{for giants,} \end{aligned} \quad (\text{A2})$$

$$\begin{aligned} I - J &= 0.141 M_V - 0.159 & \text{for dwarfs,} \\ &= -0.556 M_V + 0.944 & \text{for giants.} \end{aligned} \quad (\text{A3})$$

Since  $V - J = M_V - M_J$  we have  $M_V$  as a function of  $M_J$  which when substituted into the  $I - J$  relations with  $M_J = J - 14.5$ , where 14.5 is the distance modulus for the center of the Galaxy, yields  $I - J$  as a function of  $J$ :

$$\begin{aligned} I - J &= 0.221 J - 3.456 & \text{for dwarfs,} \\ &= -0.196 J + 3.263 & \text{for giants.} \end{aligned} \quad (\text{A4})$$

We solve each of Eqs. (A4) for  $J(I)$ . Then the LF in  $I$ -band is given by  $f_L(I) = f_L[J(I)](dJ/dI)$ . However, the range of  $I$  for each segment differs from the range in  $J$ ;  $J = 9, 17, 18, 24 \rightarrow I = 10.60, 16.93, 18.52, 25.85$ . We have assumed the expressions for the giants apply for  $9 \leq J \leq 17$  and the expressions for the dwarfs apply for  $18 \leq J \leq 24$ . We round the values of  $I$  corresponding to the segment boundaries in  $J$  slightly and assume the giant relations apply for  $10.5 \leq I \leq 17$  and the dwarf relations for  $18.5 \leq I \leq 26$ . The giant and dwarf segments are connected with a straight line in the  $I$ -band equivalent of Fig. 12 of Zoccali *et al.* (1999) and the LF renormalized so that

$$f_L(I) = 1.470 \times 10^{-9} e^{0.930 I_s}, \quad 10.5 \leq I_s \leq 17$$

$$\begin{aligned}
&= 2.575 \times 10^{-8} e^{0.762 I_8}, \quad 17 \leq I_8 \leq 18.5 \\
&= 1.316 \times 10^{-4} e^{0.300 I_8}, \quad 18.5 \leq I_8 \leq 26 \quad (\text{A5})
\end{aligned}$$

represents the fraction of the sources per unit  $I$  magnitude. (The subscript stands for the 8 kpc distance to the Galactic center.) The slope of the  $I$ -band luminosity function of Holtzman *et al.* (1998) for the dim stars is in reasonable agreement with the last of Eqs. (A5).

The luminosity function will be used in two ways in the determination of planetary detection probabilities: First in the  $S/N$  criterion for detection and second in the visibility of the sources. Both will involve a modification of the luminosity function to account for extinction as a function of the distance to the source. The extinction  $A_{I_8}$  to 8 kpc is about 0.76 magnitudes in Baade's window (Holtzman *et al.* 1998) but increases to about 18 toward the Galactic center.  $A_{I_8}$  will be retained as a free parameter to be adjusted for each LOS. We assume the extinction is uniformly distributed along the LOS such that the fractional change in intensity  $d\mathcal{I}/\mathcal{I} = -CdD_{OS}$  and  $\mathcal{I} = \mathcal{I}_0 e^{-CD_{OS}}$ , where  $D_{OS}$  is the distance to the source and  $C$  is constant. Then  $e^{-CD_{OS}} = 10^{-0.4A_I} = e^{-0.921A_I}$  yields  $CD_{OS} = 0.921A_I = CD_8\zeta = 0.921A_{I_8}\zeta$  or the extinction  $A_I = A_{I_8}\zeta$ . The apparent magnitude of a star at arbitrary  $\zeta$  along a LOS where the extinction to 8 kpc is  $A_{I_8}$  is then

$$I = I_8 + A_{I_8}\zeta + 5 \log \zeta. \quad (\text{A6})$$

For the visibility of the sources it is convenient to express the luminosity function in terms of luminosity instead of magnitudes, so we proceed to determine the  $I$ -band luminosities of the bulge stars. The  $I$ -band is centered near  $0.80 \mu\text{m}$ , with a flux density at the Earth from a 0 magnitude star like Vega of  $1.20 \times 10^{-12} \text{W cm}^{-2} \mu\text{m}^{-1}$  (McLean, 1997). The Gunn  $I$  filter spans  $0.75$  to  $0.88 \mu\text{m}$  (FWHM) ([http://ftp.noao.edu/kpno/filters/4inch\\_list.html](http://ftp.noao.edu/kpno/filters/4inch_list.html)), so the flux density in  $I$  band from Vega is  $1.56 \times 10^{-6} \text{ergs cm}^{-2} \text{sec}^{-1}$ . Then,

$$\frac{L_I}{L_\odot} = 3.06 \times 10^6 10^{-0.4I_8} = 3.06 \times 10^6 e^{-0.921I_8} \quad (\text{A7})$$

is the luminosity of a star at the Galactic center whose  $I$  magnitude is  $I_8$ .

The fraction of stars with  $L_I > L_{I_0}$  is the fraction of stars with  $I_8 < I_{80}$ , which is found by integrating

Eq. (A5) from the minimum  $I_8$  value of 10.5 to  $I_{80}$ . The latter fraction is

$$\begin{aligned}
F(I_8 < I_{80}) &= 1.581 \times 10^{-9} e^{0.930I_{80}} - 2.75 \times 10^{-5} \\
&\quad 10.5 \leq I_{80} \leq 17 \\
&= 3.381 \times 10^{-8} e^{0.762I_{80}} - 2.590 \times 10^{-3} \\
&\quad 17 \leq I_{80} \leq 18.5 \\
&= 4.387 \times 10^{-4} e^{0.300I_{80}} - 0.0711 \\
&\quad 18.5 \leq I_{80} \leq 26 \quad (\text{A8})
\end{aligned}$$

Using Eq. (A7) to convert  $I_8$  to  $L_I$ , we find the fraction of stars with  $L_I > L_{I_0}$  to be

$$\begin{aligned}
F(L_I > L_{I_0}) &= 5.64 \times 10^{-3} L_{I_0}^{-1.01} - 2.75 \times 10^{-5}, \\
&\quad 194 > L_{I_0} > 0.487, \\
&= 7.84 \times 10^{-3} L_{I_0}^{-0.827} - 2.59 \times 10^{-3}, \\
&\quad 0.487 > L_{I_0} > 0.123, \\
&= 5.71 \times 10^{-2} L_{I_0}^{-0.326} - 0.0711, \\
&\quad 0.123 > L_{I_0} > 1.23 \times 10^{-4}, \quad (\text{A9})
\end{aligned}$$

where  $L_I$  and  $L_{I_0}$  are in units of  $L_\odot$ .

### Source Visibility

We modify the cumulative luminosity function of Eqs. (A9) with extinction to determine the visibility of the sources to be monitored in a microlensing survey. The flux density received from a source at  $\zeta$  is

$$\mathcal{F} = \frac{L}{4\pi D_8^2 \zeta^2} e^{-0.921A_{I_8}\zeta}. \quad (\text{A10})$$

The fraction of sources with  $L_I > L_{I_0}$  in Eqs. (A9) has the form  $C_1 L_{I_0}^\beta + C_2$ . If  $\mathcal{F}_0$  is the minimum flux density that can be reliably monitored in a planet search from a source at  $D_{OS}$ , the cumulative luminosity function takes the form

$$\begin{aligned}
F(\mathcal{F} > \mathcal{F}_0) &= \xi(\mathcal{F}_0, \zeta, A_{I_8}) \quad (\text{A11}) \\
&= C_1 (4\pi D_8^2 \mathcal{F}_0 \zeta^2 e^{0.921A_{I_8}\zeta})^\beta + C_2.
\end{aligned}$$

Eq. (A11) represents the fraction of sources that are visible at distance  $\zeta$ .

Although beyond current practice (P. Sackett, private communication, 2000), we shall assume a source with  $I = 21$  can be monitored successfully from the ground in planet searches. This corresponds to the minimum usable flux density of  $\mathcal{F}_0 \rightarrow \mathcal{F}_{21} = 6.21 \times 10^{-15} \text{ergs cm}^{-2} \text{sec}^{-1}$ . For the  $I$  band LF that we have adopted, about 1.16% of the stars have  $I_8 < 17$  and about 4.18% have  $I_8 < 18.5$ . These are the points

in the LF where the slope changes, so the values of  $C_1, C_2, \beta$  must change for  $F$  in Eq. (A11) when  $F = 0.0116$  and  $0.0418$ . Of course  $F = 1$  for sufficiently small values of  $\zeta$  where all of the stars are visible, and  $F = 0$  for sufficiently large values of  $\zeta$  where no stars are visible, where “visible” here means  $I < 21$ . For example, substitution of the values of the constants from Eqs. (A9) along with the value of  $\mathcal{F}_{21}$  into Eq. (A11) yields

$$\begin{aligned}
F(\mathcal{F} > \mathcal{F}_{21}) &= \xi(\mathcal{F}_0, \zeta, A_{I8}) \\
&= 1, & \zeta < 0.0892, \\
&= 0.240 (\zeta^2 e^{0.921 A_{I8} \zeta})^{-0.326} - 0.0711, \\
& & 0.0892 < \zeta < 0.9075, \\
&= 0.300 (\zeta^2 e^{0.921 A_{I8} \zeta})^{-0.827} - .000259, \\
& & 0.9075 < \zeta < 1.2025, \\
&= 0.482 (\zeta^2 e^{0.921 A_{I8} \zeta})^{-1.010} - .0000275, \\
& & 1.2025 < \zeta < 2.7677, \\
&= 0, & 2.7677 < \zeta
\end{aligned} \tag{A12}$$

as the fraction of sources visible at distance  $\zeta$  for  $A_{I8} = 3$ . For  $A_{I8} = 1$  the expressions are identical to those in Eqs. (A12) except the breaks occur at  $\zeta = 0.0965, 1.5536, 2.2477$ , and  $6.4602$ . In this latter case the most luminous star in the LF could be seen far beyond the opposite edge of the Galaxy even if the absorption were to persist all along the line of sight. For  $A_{I8} = 5$  the breaks are at  $\zeta = 0.0833, 0.6739, 0.8648$  and  $1.8384$ . Fig. 13 shows the fraction of visible sources ( $I < 21$ ) as a function of  $\zeta$  for three values of  $A_{I8}$ .

## B. Amplification of the source

We adopt the analysis of Witt (1990) to determine the amplification of a point source star (source) by the star-planet binary lens as a function of the relative angular positions of the source, lensing star of mass  $M$  (hereinafter, the lens) and the planet  $m$ . However, since  $M \gg m$ , we choose the optical axis to pass through the lens and locate source and planet relative to this axis. All displacements of the projected positions on the lens plane are normalized by the Einstein ring radius of  $M$ ,  $R_E = \sqrt{4GM D_{OL}(D_{OS} - D_{OL})/(c^2 D_{OS})}$ , where  $G$  is the gravitational constant,  $c$  is the velocity of light and  $D_{OL}$  and  $D_{OS}$  are the observer-lens and observer-source distances respectively. ( $R_E$  is the radius of

the axially symmetric ring image of a source that is directly behind the lens.) The lens equation is then written

$$\lambda = w - \frac{1}{w^*} + \frac{\epsilon}{\rho^* - w^*}, \tag{B1}$$

where  $\lambda = \xi + i\eta$  and  $w = x + iy$  are the displacements of the source and image from the optical axis respectively,  $\rho = \rho_x + i\rho_y$  is the displacement of the planet and  $\epsilon = q$ . The (\*) indicates complex conjugation.  $\lambda, w, \rho$  may be interpreted as either the projected displacements in the lens plane normalized by  $R_E$  or the angular displacements normalized by the angle subtended by  $R_E$ . The axes  $(\xi, \eta)$  and  $(x, y)$  are aligned.

If we multiply the complex conjugate of Eq. (B1) by the product  $w(\rho - w)$  and substitute  $w$  as a function of  $w^*$  from Eq. (B1), the following polynomial results:

$$P(w^*) = a_5 w^{*5} + a_4 w^{*4} + a_3 w^{*3} + a_2 w^{*2} + a_1 w^* + a_0 = 0, \tag{B2}$$

where

$$\begin{aligned}
a_5 &= \lambda(\lambda - \rho) \\
a_4 &= \lambda(\lambda(-\lambda^* - 2\rho^*) + \rho\lambda^* + 2\rho\rho^* + 1 + \epsilon) - \epsilon\rho \\
a_3 &= \lambda^*(\lambda(2\rho^*\lambda - 2(1 + \epsilon) - 2\rho\rho^*) + \rho(1 + \epsilon)) \\
& \quad + \lambda(\lambda\rho^{*2} - \rho\rho^{*2} - 2\rho^*) + \epsilon\rho\rho^* \\
a_2 &= \lambda^*(\lambda(-\rho^{*2}\lambda + \rho^*(\rho\rho^* + 2\epsilon + 4)) - (2 + \epsilon)\rho\rho^* \\
& \quad - (1 + \epsilon)^2) + \lambda\rho^{*2}(1 - \epsilon) + \rho^*\epsilon(1 + \epsilon) \\
a_1 &= \lambda^*(-2\rho^{*2}\lambda + \rho^*(\rho\rho^* + 2(1 + \epsilon))) - \epsilon\rho^{*2} \\
a_0 &= -\lambda^*\rho^{*2}.
\end{aligned} \tag{B3}$$

The roots of Eq. (B2) are the complex conjugates of the positions of the images, where the number of valid images is either 3 or 5 with validity determined by substitution of the corresponding root into Eq. (B1).

Eq. (B1) represents a transformation of the coordinates of an image  $(x, y)$  to the coordinates of the source  $(\xi, \eta)$ . The amplification of the source represented by a particular image is the ratio of an element of area at the image position in the  $(x, y)$  system, as transformed from the source position in the  $(\xi, \eta)$  system, to the original element in the  $(\xi, \eta)$  system. Hence, the total amplification of the source due to the star-planet binary lens is

$$A = \sum_i |\det J_i|^{-1}, \tag{B4}$$

where (Witt, 1990)

$$\det(J) = \frac{\partial \xi}{\partial x} \frac{\partial \eta}{\partial y} - \frac{\partial \xi}{\partial y} \frac{\partial \eta}{\partial x}$$

$$\begin{aligned}
&= \left( \frac{\partial \lambda}{\partial w} \right)^2 - \frac{\partial \lambda}{\partial w^*} \left( \frac{\partial \lambda}{\partial w^*} \right)^* \\
&= 1 - \left| \frac{1}{w^{*2}} + \frac{\epsilon}{(\rho^* - w^*)^2} \right|^2 \quad (\text{B5})
\end{aligned}$$

is the determinant of the Jacobian of the transformation represented by Eq. (B1), and  $J_i = J(w_i)$  is the Jacobian evaluated at the coordinates of the  $i$ th image. The sum is over either three or five images. For a single lens without the planet the amplification simplifies to

$$A_0 = \frac{u^2 + 2}{u\sqrt{u^2 + 4}}, \quad (\text{B6})$$

where  $u$  is the angular separation of the lens and source normalized by the angle subtended by the Einstein ring radius in the lens plane.

The curves defined in  $w$  space by  $\det J = 0$  are called the critical curves where the amplification is formally infinite. This singularity is removed when the finite size of the source is considered. The corresponding closed curves in  $\lambda$  space found from Eq. (B1) are the caustics, such that when the source is on a caustic curve an image is on a critical curve. For the single star lens, the caustic reduces to a single point at the lens position, and the corresponding critical curve is the Einstein ring. If the source never crosses a caustic during the event there are always just three images and therefore three terms on the right-hand-side of Eq. (B4). At the first caustic crossing, an image is created on the critical curve and separates into two images for a total of 5 images that persist as long as the source is inside the closed caustic curve. On the second caustic crossing, with the source now outside the closed caustic, one of images created at the first crossing merges with one of the original three images and disappears—leaving again only three images.

To evaluate contours of equal amplification for a given position of the source, the amplification is evaluated for a  $401 \times 401$  grid of planet positions centered on the lens and extending  $\pm 2.5R_E$  in both orthogonal directions. A  $401 \times 401$  array of the fractional change in the amplification due to the planet,  $A/A_0 - 1$ , is saved, where  $A$  is the amplification for a particular position of the planet and  $A_0$  is the unperturbed amplification for the given source position. Contours of constant fractional change in the amplification (the perturbation due to the planet) are obtained with any contouring program for arbitrary fractional changes. In Fig. 2, the contours shown correspond to the assumed minimal perturbation that can be detected ac-

ording to the  $S/N$  at that position on the light curve. However, these contours are not used to trace their extremes along the line containing the source and lens during the course of the event.

It is more efficient to determine these extremes directly by moving the planet along the axis containing the source and lens to determine the two points on opposite sides of each unperturbed image position where the fractional change in the amplification is  $2/(S/N)$  for the major image outside  $R_E$  and  $-2/(S/N)$  for the minor image inside  $R_E$ . The lens-source line is chosen to be the real axis so that  $\lambda = \lambda^*$  and  $\rho = \rho^*$ . The coefficients in Eq. (B3) are then real and analytic in  $\rho$ , which is now the linear position of the planet along the real axis. We form the function

$$f(\rho) = \frac{A}{A_0} - \frac{1}{A_0} \sum_i |\det(J_i)|^{-1}, \quad (\text{B7})$$

where  $A = A_0[1 \pm 2/(S/N)]$  defines the extremes of the planet positions along the real axis on either side of the unperturbed image positions inside of which the fractional perturbation would exceed  $2/(S/N)$  and allow detection of the planet. These extremes are defined by the zeros of  $f(\rho)$ . A trial value of  $\rho$  somewhat removed from the unperturbed position of a real image is used to start a “safe” Newton’s method solution for a zero of  $f(\rho)$  (Press, *et al.* 1986). All the necessary derivatives can be found from Eqs. (B2) and (B3), where  $\rho^* = \rho$  in the latter, and the realness of the coefficients is exploited. A step in the procedure is thus for a trial position of  $\rho$ , all of the valid roots of the polynomial form of the lens equation (Eq. (B2)) are used to form  $f(\rho)$  and  $df(\rho)/d\rho$  for use in Newton’s method to determine the next approximation to the root, where the procedure is iterated until a tolerable precision is obtained. The two pairs of roots are determined for each position of the source as it is stepped through the event, where  $S/N$  is a function of the source position.

### C. Probability distribution of projected star-planet separation

If  $dn_L(M, D_{OL})/dM$  is the number density of stars (lenses) per unit mass interval near mass  $M$  and near distance  $D_{OL}$ , then  $(dn_L(M, D_{OL})/dM)D_{OL}^2 dD_{OL} dM \Delta\Omega$  is the number of stars in mass range  $dM$  about  $M$  and in volume  $D_{OL}^2 dD_{OL} \Delta\Omega$ , where  $\Delta\Omega$  is a representative solid angle in the telescope field of view. The fraction

of the lenses in the volume of those along the LOS to the source is just this quantity divided by its integral along the LOS and over the mass function, where we assume the MF to be spatially invariant. Hence,

$$F(x_p, a, \zeta) = \int_0^\zeta \int_{M_{min}}^{M_{max}} F(x_p, a, \zeta, z, M) \Theta \left[ \frac{a^2 \zeta}{KMz(\zeta - z)} - x_p^2 \right] \times z^2 \frac{dn_L(M, z)}{dM} dM dz / \int_0^\zeta \int_{M_{min}}^{M_{max}} z^2 \frac{dn_L(M, z)}{dM} dM dz \quad (C1)$$

is the average of  $F(x_p, a, \zeta, z, M)$  over the lens distribution from observer to source and over the MF. We have normalized the distances with  $D_8$  as above and introduced the step function  $\Theta(x)$  to exclude those regions of  $z, M$  space for which the integrand in the numerator is undefined. If  $x_p^2 > a^2 \zeta / (KMz(\zeta - z))$ ,  $r > a$  in Eq. (6). For fixed  $x_p$  and  $a$ , Eq. (C1) represents the average of  $F(x_p, a, \zeta, z, M)$  over those lenses distributed along the LOS to distance  $\zeta$  for which  $R_E < a/x_p$ .

For the density distribution in the Galaxy we adopt the double exponential model for the disk distribution of mass and a triaxial bar distribution for the bulge. The disk model is that of Bahcall and Soneira (1980),

$$\rho_M = \int_{M_{min}}^{M_{max}} \frac{d\rho}{dM} dM = \rho_{M0} \exp \left( \frac{-|z'|}{300 \text{pc}} - \frac{r}{s_d} \right), \quad (C2)$$

where  $z'$  is the coordinate perpendicular to the plane of the galaxy,  $r$  is the radial coordinate in the plane of the galaxy, and  $s_d = 2.7$  kpc is the scale length in the radial direction, which is chosen less than the 3.5 kpc used by Bahcall and Soneira (Zhao, Spergel & Rich 1995; Kent, Dame & Fasio 1995), and where  $\rho_{M0}$  is chosen such that  $\rho_M = 0.05 M_\odot / \text{pc}^3$  at  $z' = 0$  and  $r = 8$  kpc. Like Zhao, Rich and Spergel (1996), we choose the triaxial bulge model of Zhao (1996) but keep the nucleus in a truncated form and do not terminate the bulge at 3.3 kpc:

$$\rho_M = \rho_0 \left[ \exp \left( -\frac{s_b^2}{2} \right) + s_a^{-1.85} \exp(-s_a) \right], \quad (C3)$$

where

$$s_b^4 = \left[ \left( \frac{x}{\sigma_x} \right)^2 + \left( \frac{y}{\sigma_y} \right)^2 \right]^2 + \left( \frac{z'}{\sigma_z} \right)^4,$$

$$s_a^2 = \frac{q_a^2(x^2 + y^2) + z'^2}{\sigma_z^2} \quad \text{if } \sqrt{x^2 + y^2} > 0.56 \text{ kpc}, \\ = \frac{0.3136 q_a^2 + z'^2}{\sigma_z^2} \quad \text{if } \sqrt{x^2 + y^2} \leq 0.56 \text{ kpc} \quad (C4)$$

with  $q_a = 0.6$ ,  $\sigma_x = 1.49$  kpc,  $\sigma_y = 0.58$  kpc, and  $\sigma_z = 0.40$  kpc. The coefficient  $\rho_0$  determines the mass of the bulge. The nucleus is truncated to avoid the singularity at the origin in the Zhao bulge model. The observations are consistent with the long axis of the bulge inclined about  $13^\circ$  to  $20^\circ$  relative to the LOS to the Galactic center with the near side of the bar lying in the second quadrant. We shall choose  $\theta = -13^\circ$ , but note that this angle is very uncertain.

The origin of coordinates for both disk and bulge distributions is transferred from the Galactic center to the position of the observer with the following transformation:

$$x = \cos \theta - z \cos b \cos(\ell - \theta), \\ y = -\sin \theta - z \cos b \sin(\ell - \theta), \\ z' = z \sin b, \quad (C5)$$

for a lens in the bulge where  $z$  is the distance along the line of sight normalized by  $D_8$  with  $xyz'$  being galactocentric coordinates along the bulge principal axes normalized by  $D_8$  and  $\theta$  the inclination of the bulge axis to the line between the observer and the Galactic center measured in the direction of increasing  $\ell$ . For the disk distribution, the transformation is

$$r^2 = 1 + z^2 \cos^2 b - 2z \cos b \cos \ell, \\ z' = z \sin b, \quad (C6)$$

For a dynamically constrained bulge mass of  $2.2 \times 10^{10} M_\odot$  (Zhao, 1996),  $\rho_0$  in Eq. (C3) is  $2.5 M_\odot \text{pc}^{-3}$ . The coefficient  $\rho_{M0} = 0.05 e^{8/s_d} M_\odot \text{pc}^{-3}$  ( $s_d$  in kpc) in Eq. (C2) to satisfy the constraint on the local mass density. The conversion of these mass distributions to number density distributions for use in  $dn_L/dM$  depends on the assumed mass function. We shall adopt the Holtzman *et al.* (1998) MF for both disk and bulge stars given by

$$\phi(M) = 0.7795 M^{-1} \quad 0.08 \leq M \leq 0.7 \\ = 0.5081 M^{-2.2} \quad 0.7 \leq M \leq 2.0 \quad (C7)$$

The MF in Eq. (C7) is defined so that  $M\phi(M)dM$  represents the mass of stars/ $\text{pc}^3$  in mass range  $dM$  about  $M$  normalized such that the total mass density

is  $1M_{\odot}\text{pc}^{-3}$ . A more recent MF (Zocalli *et al.* 2000) has an index of 1.3 instead of 1 in the M star region. However, we use the Holtzman *et al.* MF and point out the effects of increasing the index for small mass stars in Fig. 17. We truncate the MF at  $2M_{\odot}$  because of the small number of stars of higher mass. We could extend the MF into the brown dwarf region, but the microlensing event time scale frequency distribution does not seem compatible with a large number of brown dwarfs—at least in the Galactic bulge (Peale, 1999).

The number of stars/ $M_{\odot}$ , or equivalently, stars/ $\text{pc}^3$  for this assumed MF is found from integration of Eq. (C7) to be 2.1562 stars/ $M_{\odot}$ , so the number density of stars corresponding to the mass densities given by Eqs. (C2) and (C3) are found by multiplying each by this factor. The expression for  $dn_L/dM$  is the sum of the disk and bulge contributions at a given point, so

$$\begin{aligned} dn_L(M, z)/dM &= \\ &0.7795[0.1078e^A + 5.3903(e^{-\frac{s_b^2}{2}} + s_a^{-1.85}e^{-s_a})]/M, \\ &0.08 < M < 0.7 \\ &= 0.5081[0.1078e^A + 5.3903(e^{-\frac{s_b^2}{2}} + s_a^{-1.85}e^{-s_a})]/M^{2.2}, \\ &0.7 < M < 2.0 \end{aligned} \tag{C8}$$

where  $A$  is the exponent given in Eq. (C2)  $+8/s_d$  but with the change of coordinates given in Eqs. (C6) and (C5) in all of  $A$ ,  $s_a$ , and  $s_b$ . As we shall be dealing in fractional distributions, only the ratio of the coefficients of the disk and bulge distributions will have any effect on the probabilities. The integrals in Eq. (C1) are evaluated with a Monte Carlo technique (Press *et al.* 1986) as a function of  $x_p$  for given  $a$ .

## References

Albrow M, Beaulieu JP, Birch P, Caldwell AR, Kane S. *et al.* (1998) The 1995 pilot campaign of PLANET: Searching for microlensing anomalies through precise, rapid round-the-clock monitoring. *Astrophys. J.* **509**, 678-702.

Albrow MD, Beaulieu J-P, Caldwell JAR, DePoy DL, Dominik M, Gaudi BS, Gould A, Greenhill J, Hill K, Kane S, Martin R, Menzies J, Naber RM, Pogge RW, Pollard KR, Sackett PD, Sahu KC, Vermaak P, Watson R, Williams A. (2000a) Limits on Stellar and Planetary Companions in Microlensing Event OGLE-1998-BUL-14, *Astrophys. J.* **535**, 176-89.

Albrow MD, An J, Beaulieu J-P, Caldwell JAR, DePoy DL, Dopminik M, Gaudi BS, Gould A, Greenhill J, Hill K, Kane S, Martin R, Menzies J, Naber RM, Pel J-W, Pogge RW, Pollard KR, Sackett PD, Sahu KC, Vermaak P, Vreeswijk PM, Watson R, Williams A. (2000b) Limits on the abundance of galactic planets from five years of PLANET observations, astro-ph/0008078. *Astrophys. J.* In press.

Alcock C, Allsman RA, Alves DR, Axelrof TS, Becker AC, Bennett DP, Cook KH, Drake AJ, Freeman KC, Geha AM, Griest K, Lehner MJ, Marshall, SL, Minniti D, Nelson CA, Peterson BA, Popowski P, Pratt MR, Quinn PJ, Stubbs CW, Sutherland W, Tromaney AB, Vandehei T, Welch DL. (2000) The Macho project: Microlensing optical depth towards the galactic bulge from difference image analysis, astro-ph 0002510. *Astrophys. J.* In press.

Allen CW. (1973) *Astrophysical Quantities* Athone Press, Univ. of London, p. 200.

Bahcall JN, Soneira RM. (1980) The universe at faint magnitudes. I. Models for the galaxy and the predicted star counts. *Astrophys. J. Sup.* **44** 73-110.

Basu S, Rana NC. (1992) Multiplicity corrected mass function of main-sequence stars in the solar neighborhood, *Astrophys. J.* **393**, 373-84.

Beichman CA. (1996) (Ed.) A road map for the exploration of neighboring planetary systems, publication 92-22, Jet Propulsion Lab., Pasadena, CA.

Bennett DP, Rhie SH (1996) Detecting Earth-Mass Planets with Gravitational Microlensing. *Astrophys. J.* **472**, 660-64.

Bennett DP, Rhie SH (2000) The Galactic Exoplanet Survey Telescope: A proposed space-based microlensing survey for terrestrial extra-solar planets, astro-ph 0003102, In *Proceedings of the Disks, Planetesimals & Planets Meeting, Tenerife, Jan. 24-28, 2000* In press.

Bessell MS, Brett JM. (1988) JHKLM photometry: Standard systems, passbands, and intrinsic colors, *Pub. Astron. Soc. Pac.* **100**, 1134-51.

Charbonneau D, Brown TM, Latham DW, Mayor M. (2000) Detection of planetary transits across a Sun-like star. *Astrophys. J.* **529**, L45-L48.

- Frogel JA, Whitford AE. (1987) M giants in Baade's window - Infrared colors, luminosities, and implications for the stellar content of E and S0 galaxies, *Astrophys. J.* **320**, 199-237.
- Gatewood G. (1991) The Allegheny Observatory search for planetary systems, *IAF, International Astronautical Congress, 42nd*, Montreal, Canada Oct. 5-11.
- Gaudi BS, Sackett PD. (2000) Detection efficiencies of microlensing datasets for stellar and planetary companions, *Astrophys. J.* **528**, 56-73.
- Gould A, Loeb A (1992) Discovering planetary systems through gravitational microlensing, *Astrophys. J.* **396**, 104-14.
- Gould A, Bahcall J, Flynn C. (1997) M dwarfs from Hubble Space Telescope star counts. III. The Groth Strip, *Astrophys. J.* **482**, 913-18.
- Griest K, Safizadeh N. (1998) The use of high-magnification microlensing events in discovering extrasolar planets. *Astrophys. J.* **500**, 37-50.
- Henry GW, Marcy GW, Butler RP, Vogt SS. (2000) A transiting "51 Peg-like" planet, *Astrophys. J.* **529**, L41-L44
- Holtzman JA, Watson AM, Baum WA, Grillmair CJ, Groth EJ, Light RM, Lynds R, O'Neil EJ. (1998) The luminosity function and initial mass function in the Galactic bulge, *Astron. J.* **115**, 1946-57.
- Kent SM, Dame TM, Fasio G. (1991) Galactic structure from the spacelab infrared telescope 2. Luminosity models of the milky way, *Astrophys. J.* **378**, 131-38.
- Lattanzi MG, Spagna A, Sozzetti A, Casertano S. (2000) *Mon. Not. Roy. Ast. Soc.* In press.
- Mao S, Paczyński B. (1991) Gravitational microlensing by double stars and planetary systems, *Astrophys. J.* **374**, L37-L40.
- Marcy GW, Cochran WD, Mayor M. (2000) Extrasolar planets around main-sequence stars, In *Protostars and Planets IV* eds. V Mannings, AP Boss and SS Russel, Univ of Arizona Press, Tucson AZ. p. 1285.
- McLean I. (1997) *Electronic Imaging in Astronomy*, John Wiley and Sons, New York, p304.
- Peale SJ. (1997) Expectations from a microlensing search for planets, *Icarus* **127**, 269-89.
- Peale SJ. (1998) On microlensing event rates and optical depth toward the galactic center, *Astrophys. J.* **509**, 177-91.
- Peale SJ. (1999) Newly discovered brown dwarfs not seen in microlensing timescale frequency distribution? *Astrophys. J.* **524**, L67-L70.
- Press WH, Flannery BP, Teukolsky SA, Vetterling WT. *Numerical Recipes* Cambridge University Press, London, p. 221.
- Rhie SH, Becker A, Bennett DP, Calitz J, Cook K, Fragile P, Johnson B, Gurovich S, Han C, Hoffman M, Laws C, Martinez P, Meintjes P, Minniti D, Park S, Peterson B, Quinn J. (2000) Microlensing Planet Search Project, *Planetary systems in the universe, International Astronomical Union. Symp no. 202* Manchester, England , August 2000.
- Swain MR, Akeson RL, Colavita MM, Shao M. (2000) Detecting extrasolar planets with the Keck interferometer, *Planetary systems in the universe, International Astronomical Union. Symp no. 202* Manchester, England , August 2000.
- Tiede GP, Frogel JA, Terndrup DM. (1995) Implications of new JHK photometry and a deep infrared luminosity function for the Galactic bulge, *Astron. J.* **110**, 2788.
- Walker AR. (1987) *NOAO Newsletter #10*, June.
- Witt HJ. (1990) Investigation of high amplification events in light curves of gravitationally lensed quasars. *Astron. Astrophys.* **236**, 311-322.
- Zhao HS, Spergel DN, Rich RM. (1995) Microensing by the galactic bar, *Astrophys. J.* **440**, L13-L16.
- Zhao HS, Rich RM, Spergel DN. (1996) A consistent microlensing model for the galactic bar, *Mon. Not. Roy. Ast. Soc.* **282**, 175-81.
- Zhao HS. (1996) A steady state dynamical model for the COBE-detected galactic bar, *Mon. Not. Roy. Ast. Soc.* **283**, 149-66.

Zoccali M, Cassisi S, Frogel JA, Gould A, Ortolani S, Renzini A, Rich RM, Stephens AW. (2000) The initial mass function of the galactic bulge down to  $\sim 0.15M_{\odot}$ , *Astrophys. J.* **530**, 418-28.